








Cytochrome *c* levels affect the TOR pathway to regulate growth and metabolism under energy-deficient conditions

María Victoria Canal , Natanael Mansilla , Diana E. Gras , Agustín Ibarra , Carlos M. Figueroa , Daniel H. Gonzalez  and Elina Welchen 

Instituto de Agrobiotecnología del Litoral (CONICET-UNL), Facultad de Bioquímica y Ciencias Biológicas, Universidad Nacional del Litoral, 3000, Santa Fe, Argentina

Author for correspondence:
Elina Welchen
Email: ewelchen@fbcb.unl.edu.ar

Received: 31 October 2023
Accepted: 3 December 2023

New Phytologist (2024) 241: 2039–2058
doi: 10.1111/nph.19506

Key words: *Arabidopsis thaliana*, cytochrome *c*, energy deficiency, mitochondria, starvation, target of rapamycin.

Summary

- Mitochondrial function is essential for plant growth, but the mechanisms involved in adjusting growth and metabolism to changes in mitochondrial energy production are not fully understood.
- We studied plants with reduced expression of *CYTC-1*, one of two genes encoding the respiratory chain component cytochrome *c* (CYTc) in *Arabidopsis*, to understand how mitochondria communicate their status to coordinate metabolism and growth.
- Plants with CYTc deficiency show decreased mitochondrial membrane potential and lower ATP content, even when carbon sources are present. They also exhibit higher free amino acid content, induced autophagy, and increased resistance to nutritional stress caused by prolonged darkness, similar to plants with triggered starvation signals. CYTc deficiency affects target of rapamycin (TOR)-pathway activation, reducing S6 kinase (S6K) and RPS6A phosphorylation, as well as total S6K protein levels due to increased protein degradation via proteasome and autophagy. TOR overexpression restores growth and other parameters affected in *cytc-1* mutants, even if mitochondrial membrane potential and ATP levels remain low.
- We propose that CYTc-deficient plants coordinate their metabolism and energy availability by reducing TOR-pathway activation as a preventive signal to adjust growth in anticipation of energy exhaustion, thus providing a mechanism by which changes in mitochondrial activity are transduced to the rest of the cell.

Introduction

For most living organisms, respiration plays a crucial role in energy production. This process takes place in the mitochondria of eukaryotic organisms, where electrons from reduced coenzymes (NADH and FADH₂) are transported through a series of protein complexes (Complexes I–IV) to reduce oxygen. This transport is linked to ATP synthesis through the electrochemical gradient generated across the inner membrane by the action of Complexes I, III, and IV, ultimately leading to oxidative phosphorylation (OXPHOS). The plant mitochondrial electron transport chain (mETC) has some unique features, such as alternative NAD(P)H dehydrogenases and an alternative oxidase (AOX; Meyer *et al.*, 2019). Even though the alternative pathways are not directly involved in ATP production, they are essential in preventing over-reduction and blockage of the mETC, particularly during metabolic, energetic, and redox imbalance situations, such as those caused by oxidative stress. AOX uses electrons from ubiquinone to reduce oxygen, thus bypassing Complexes III and IV. This originates two possible electron pathways, the alternative and the cytochrome *c* (CYTc)-dependent pathways. Thus, the amount of ATP

produced by respiration will depend on the partition of electrons between these two pathways (Meyer *et al.*, 2019).

CYTc is a small heme protein involved in electron transport between Complexes III and IV. In addition, it performs multiple other functions as an electron carrier within and outside mitochondria (i.e. protein import into mitochondria, ascorbic acid biosynthesis, and D-lactate oxidation; Welchen & Gonzalez, 2016). While it remains uncertain whether CYTc is involved in programmed cell death in plants, it may translocate to adjacent cells through plasmodesmata after being released from mitochondria (Welchen & Gonzalez, 2021). Moreover, CYTc connects mitochondria and hormonal pathways. Thus, altered CYTc expression impacts the activity of abscisic acid (ABA) and gibberellin-regulated pathways during germination and vegetative growth, respectively. Plants with reduced CYTc levels have delayed germination and lower levels of GAs-content that are transduced in a delayed developmental transition during vegetative and reproductive life stages (Racca *et al.*, 2018, 2022).

Coordinating mitochondrial respiratory activity with nutrient provision, the cellular environment, and plant energy requirements is crucial. Cellular signals that affect mitochondrial

function are known as anterograde, while those that communicate mitochondrial status to the rest of the cell are known as retrograde signals. One of these communication pathways, known as the mitochondrial retrograde response (MRR), is regulated by the transcription factor ANAC017 (Ng *et al.*, 2014). Under normal conditions, ANAC017 remains associated with the endoplasmic reticulum membrane. However, it is translocated to the nucleus to induce MRR upon inhibiting the CYTc-dependent pathway (De Clercq *et al.*, 2013; Welchen *et al.*, 2021). In addition, some alterations in mitochondrial activity also produce the mitochondrial unfolded protein response. This response has been preferentially described in animals, but studies indicate that it also occurs in plants and is mediated by ANAC017 (Kacprzak *et al.*, 2020). In addition, hormonal signaling pathways, such as the auxin and ethylene pathways, are associated with the MRR, with the latter being independent of ANAC017 (Ivanova *et al.*, 2014; Kacprzak *et al.*, 2020).

Nutrient levels, including sugars, amino acids, nitrogen, sulfur, and phosphorus, along with metabolic balance, constitute the central regulators of growth and development (Liu *et al.*, 2021; Ingargiola *et al.*, 2023). In plants, the growth-promoting signals of Hexokinase 1 and target of rapamycin (TOR) protein kinase, the inhibitory pathway represented by the evolutionarily conserved sucrose nonfermenting-related Kinase 1 (SnRK1), and the regulatory effects of critical metabolites such as trehalose 6-phosphate converge to achieve this balance (Sheen, 2014; Figueroa & Lunn, 2016; Baena-González & Hanson, 2017).

The TOR pathway affects plant development throughout different stages of the life cycle. It promotes ribosome biogenesis, protein translation, and metabolic activation, ensuring cell cycle progression, meristem activation, organ development, cotyledon opening, and growth (Dobrenel *et al.*, 2016; Shi *et al.*, 2018; Van Leene *et al.*, 2019). Mutations in TOR-pathway components can cause embryonic lethality (Deprost *et al.*, 2007) or delayed germination and reduced seed viability (Salem *et al.*, 2017). TOR coordinates light perception and hormone levels to ensure seedling growth and development (Chen *et al.*, 2018; Schepetilnikov & Ryabova, 2018). It also controls cell proliferation in the root and shoot apical meristems (Li *et al.*, 2017). Autophagy is also regulated by TOR and depends on soluble sugars and brassinosteroid levels (Dobrenel *et al.*, 2016; Liao *et al.*, 2023). The signaling pathway mediated by TOR responds to changes in nutrient concentrations and amino acid levels that impact respiratory and energetic metabolism (Caldana *et al.*, 2013; Cao *et al.*, 2019; O'Leary *et al.*, 2020).

Previously, we reported that a complete CYTc deficiency leads to embryo lethality (Welchen *et al.*, 2012). Arabidopsis plants with reduced expression of both genes encoding CYTc – knockdown for *CYTC-1* (At1g22840) and knockout for *CYTC-2* (At4g10040) – show growth defects, including delayed germination and developmental transitions (Racca *et al.*, 2018, 2022). In this work, we describe that the alterations observed in CYTc-deficient plants are related to changes in the TOR-pathway activity, hinting at the existence of a mitochondrial signal to adjust growth and metabolism according to energy availability to avoid affecting essential cellular processes under nonoptimal energetic conditions.

Materials and Methods

Plant materials

Plants used in this study were in the *Arabidopsis thaliana* (L.) Heynh. ecotype Columbia (Col-0) background. T-DNA insertion mutants in *CYTC-1* (At1g22840; GK586B10 and SALK_143142) and double mutants in *CYTC-1* and *CYTC-2* (At4g10040; *cytc-1b2a* and *cytc-1b2b*) were described in Welchen *et al.* (2012). The *CYTC-1* overexpressing line (oeCYTc) was obtained and described previously in Racca *et al.* (2018). Autophagic mutant plants in *ATG5* (At5g17290; SAIL_129_B07) and *ATG7* (At5g45900; GABI_655_B06), and the TOR-pathway mutants *raptor1b* (At3g08850; SALK_078159), *rps6b* (At5g10360; SALK_012147C), and *lst8* (At3g18140; SALK_012147C) were obtained from the Arabidopsis Biological Resource Center (ABRC, Ohio State University, USA). The Arabidopsis plant line overexpressing S6 kinase (S6K; At3g08730) fused to the HA tag (35S::S6K-HA) was kindly provided by Dr. Jen Sheen (Department of Molecular Biology – Massachusetts General Hospital, Boston, USA). A line overexpressing TOR (At1g50030) fused to GFP (35S::GFP-TOR; Schepetilnikov *et al.*, 2017) was kindly donated by Dr Lyuba Ryabova (Institut de Biologie Moléculaire des Plantes, Strasbourg, France), and the ATG8a (At4g21980) overexpressing line fused to GFP (35S::GFP-ATG8a; Thompson *et al.*, 2005) was kindly provided by Dr Pablo Manavella (IAL, Santa Fe, Argentina).

Growth conditions

For chemical treatments and western blot analysis, seedlings were grown for 3.5 d in ½-strength Murashige & Skoog (½MS) liquid medium, followed by an extended night (16 h) for nutrient depletion. Then, seedlings were treated with 20 mM glucose or sucrose, according to Li *et al.* (2017) and Xiong *et al.* (2013), for different periods, as indicated in each figure. The photoperiod was long day (LD; 16 h : 8 h, light : dark) at an intensity of 100 $\mu\text{mol m}^{-2} \text{s}^{-1}$ and a 22–24°C. Seedlings for phenotypic analysis were grown in vertical plates with MS medium containing 1% (w/v) agar, under the same conditions of light and temperature indicated above.

Starvation assay

Seedlings were grown for 3.5 d in ½MS liquid medium followed by an extended night (16 h) for nutrient depletion and then treated for 3 extra days with 20 mM sucrose to induce growth. After that, half of the plants were kept on sucrose, and the other half were placed in darkness without sucrose to induce starvation. At specified time points, samples were collected to measure chlorophyll content, which served as an indicator of sensitivity to carbon stress.

Chemical treatments

For chemical treatments, seedlings were grown according to the protocol described in Xiong *et al.* (2013) and treated with

the uncoupling agent 2–4 dinitrophenol (2–4 DNP) at a final concentration of 1 μM for 72 h, antimycin A (AMA) at 5 μM for 48 h, or AZD-8055 at 0.5 μM and 1 μM for 48 h.

Staining and confocal microscopy

The reporter line 35S::GFP-ATG8a was used for autophagy analysis through confocal microscopy. The excitation and detection wavelengths were set at 488 and 498–531 nm, respectively. The images were acquired using a Leica TCS SP8 confocal microscope and a $\times 20$ dry objective. Original images were used to quantify the number of autophagosomes with Fiji software. All images were captured at the outermost root layer. Alternatively, roots were stained with 1 μM LysoTracker™ Green DND-26 (Invitrogen) for 15 min and then washed twice for 5 min with distilled water. LysoTracker fluorescence was analyzed using the same excitation and detection parameters as described for 35S::GFP-ATG8a. Tetramethylrhodamine methyl ester (TMRM; 1 μM) was used to evaluate mitochondrial membrane potential. MitoTracker™ Green FM (Invitrogen) at the same concentration was used as a control of total mitochondrial mass/number. The roots were stained for 20 min, followed by a single wash with distilled water for 5 min. Excitation and detection wavelengths were 488 nm/498–531 nm for MitoTracker and 552 nm/590–620 nm for TMRM. Images were acquired with a $\times 63$ water immersion objective. The ‘mean gray value’ parameter (the mean fluorescence intensity per unit root area) calculated by the Fiji software, was used for quantification.

ATP measurements

Adenylates were extracted as described by Raveneau *et al.* (2017). Briefly, 50 mg of seedlings were homogenized with 400 μl of methanol : chloroform (1 : 1), and phase separation was triggered by adding 250 μl H_2O . After centrifugation, the aqueous phase was used for adenylate quantification by high-performance liquid chromatography (HPLC), as described by Menegollo *et al.* (2019). Samples (10 μl) were injected onto a Luna Omega C18 column (Phenomenex, Torrance, CA, USA, particle size 3 μm , 150 \times 4.6 mm) equipped with a PS C18 SecurityGuard cartridge (Phenomenex) and connected to a Prominence-i LC-2030C Plus system (Shimadzu, Kyoto, Japan). Separation was performed at 30°C with a flow rate of 0.75 ml min^{-1} and a mobile phase of 0.1 M $\text{NH}_4\text{H}_2\text{PO}_4$, pH 6.0, and 1% (v/v) methanol. The peak corresponding to ATP was identified by spiking samples with a standard compound (Sigma-Aldrich). Quantification was performed with a standard curve of known concentrations and the LABSOLUTIONS LITE software (Shimadzu) using the absorbance at 254 nm.

Extraction and determination of chlorophylls, carbohydrates, and total amino acids

A total of 20 mg of fresh seedlings were used to determine the chlorophylls, soluble sugars (glucose, sucrose, and fructose), and amino acid content. The samples were collected in Eppendorf

tubes, frozen, and disaggregated in liquid nitrogen. The extraction was performed by resuspending the tissue in 250 μl of 80% ethanol in 10 mM HEPES-KOH (pH 7.0) and incubating it for 20 min at 80°C. Subsequently, the mixture was centrifuged at 12 000 g for 10 min. The resulting supernatant was carefully transferred to a new tube (S1), while the pellet was resuspended in 250 μl of 50% ethanol in 10 mM HEPES-KOH (pH 7.0). This resuspension was then incubated at 80°C and centrifuged at 12 000 g for 10 min. The supernatant obtained (S2) was combined with S1. Next, the pellet was resuspended in 150 μl of 80% ethanol in 10 mM HEPES-KOH (pH 7.0), followed by incubation at 80°C and centrifugation at 12 000 g for 10 min. The resulting supernatant (S3) was added to the combined S1 and S2 supernatants, and an aliquot was used to determine the different metabolites. The pellet was saved to quantify the starch content.

The chlorophylls were determined by measuring the absorbance at 645 and 665 nm in a microplate of 96 wells from 50 μl of the ethanolic extract diluted with 120 μl of absolute ethanol. The following formula was used to calculate the amount of Chl *a* and Chl *b*:

$$\text{Chl } a \text{ (}\mu\text{g per well)} = 5.48A_{665} - 2.16A_{645}$$

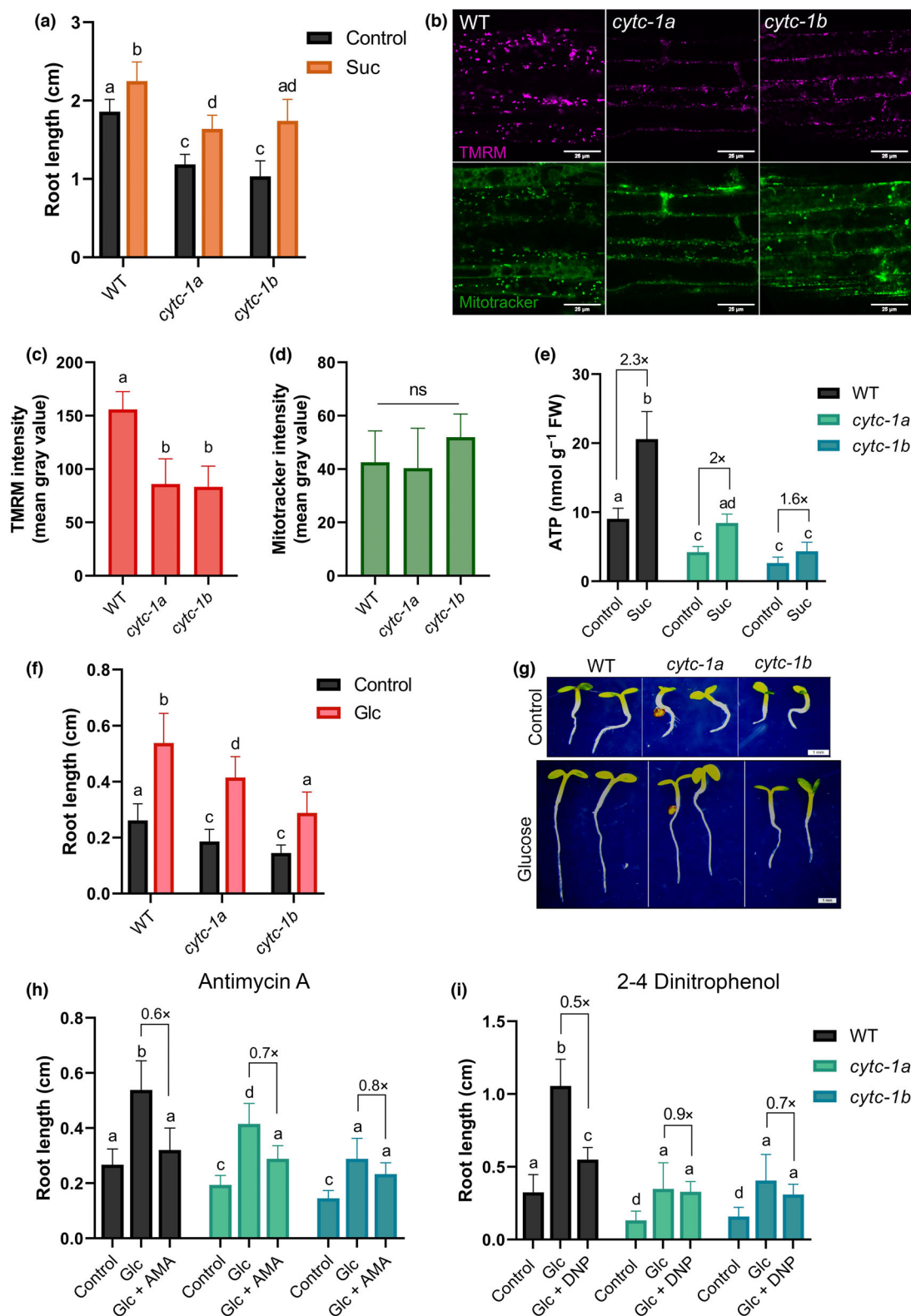
$$\text{Chl } b \text{ (}\mu\text{g per well)} = 9.67A_{645} - 3.04A_{665}$$

The content of soluble sugars was determined from an aliquot of the ethanolic extract with an enzymatic method following the protocol developed by Stitt *et al.* (1989).

Total amino acid content was determined using a fluorescence method with fluorescamine (F9015, Sigma) and quantified using a standard curve of glutamate. The protocol was described by Bantan-Polak *et al.* (2001) with excitation and emission wavelengths set at 405 and 485 nm, respectively. The pellet saved in the ethanolic extraction was treated with amyloglucosidase and α -amylase to hydrolyze the starch. Starch content was quantified with an enzymatic method according to Hendriks *et al.* (2003).

Amino acid quantification by HPLC

The amino acid profile was quantified by HPLC using the ethanolic extract described in the previous section. Samples (1 μl) were injected into the same column and system described for ATP determination. The co-injection method was applied using the o-Phthaldialdehyde and mercaptopropionic acid reagents to generate the derivative compounds with excitation and emission wavelengths set at 350 and 450 nm, respectively. Separation was performed at 40°C with a flow rate of 0.75 ml min^{-1} , using a mobile phase A (15 mM potassium dihydrogenphosphate/5 mM dipotassium hydrogen phosphate) and mobile phase B (water : acetonitrile : methanol 15 : 45 : 40). Peaks corresponding to each amino acid were identified by using a standard solution with known concentrations (A2161, Sigma). Quantification was performed with a standard curve of known concentrations and the LABSOLUTIONS LITE software (Shimadzu).



Total RNA extraction and real-time qPCR analysis

RNA extraction, cDNA synthesis, and gene expression analysis by RT-qPCR were performed as described in Welchen *et al.* (2012). Transcript levels were measured by reverse

transcription followed by quantitative polymerase chain reaction (RT-qPCR) of tissue-specific total RNA. Samples were collected, frozen in liquid nitrogen, and stored at -80°C until use. Total RNA was prepared using TRIzol reagent followed by a LiCl precipitation step. Reverse transcription was performed on

Fig. 1 Root growth and mitochondrial activity are affected in *CYTC-1* deficient plants. (a) Root length (cm) measured in 6-d-old wild-type (WT), *cytc1-a*, and *cytc1-b* mutant plants grown in vertical plates with $\frac{1}{2}$ -strength Murashige & Skoog ($\frac{1}{2}$ MS) medium containing 1% agar without the addition of carbon source (black bars: Control), or with 1% (w/v) sucrose (orange bars: Suc), in a long-day (LD) diurnal cycle. Bars represent the mean (\pm SD) of root length for plants grown without sugar addition (black bars: Control) or in the presence of sucrose (orange bars: Suc). Different letters indicate significant differences based on Sidak's multiple comparisons tests ($n > 15$, $P < 0.05$). (b) Representative images acquired by confocal microscopy of mitochondria from root cells of 5-d-old WT and mutant (*cytc-1a* and *cytc-1b*) seedlings grown in vertical plates with $\frac{1}{2}$ MS medium containing 1% (w/v) agar and stained with 1 μ M tetramethylrhodamine methyl ester (TMRM; upper panel) or 1 μ M MitoTracker Green (lower panel). Bars, 25 μ m. (c, d) Quantification of the intensity of mitochondrial fluorescence detected in the images of plants stained with TMRM (c) and Mitotracker Green (d). Bars represent the mean (\pm SD) of the mean gray value, analyzed per unit root area with Fiji software. Different letters indicate significant differences based on Tukey's test ($n > 10$ roots, $P < 0.05$), ns, not significant. (e) Quantification of ATP content (nmol mg^{-1} FW) measured by HPLC in seedlings grown for 3.5 d in MS liquid medium, followed by an extended night for nutrient depletion (16 h darkness) and exposed to 90 mM sucrose in darkness for 3 h (Suc). The control condition corresponds to seedlings kept under the same condition without sugar addition. Different letters indicate significant differences based on Sidak's multiple comparisons tests ($n = 3$ biological replicates, $P < 0.05$). (f) Root growth response of the WT and *cytc-1* mutants to sugar in the growth medium. Seedlings were grown for 3.5 d in MS liquid medium in a LD diurnal cycle, followed by an extended night for nutrient depletion (16 h darkness). Then, glucose was added to 20 mM final concentration, and root length was measured after incubation for 24 h in light. Bars represent the mean (\pm SD) of root length for plants grown without the addition of glucose (black bars: Control) or in the presence of glucose (pink bars: Glc). Different letters indicate significant differences based on Sidak's multiple comparisons tests ($n > 15$, $P < 0.05$). (g) Representative images of WT and single mutant seedlings (*cytc-1a* and *cytc-1b*) grown as in (f). Bars, 1 mm. (h, i) Root length (cm) measured in the presence of the mitochondrial electron transport chain inhibitor antimycin A (AMA, 1 μ M) for 48 h (h) or the uncoupler 2,4-dinitrophenol (DNP, 50 μ M) for 72 h (i). WT and mutant (*cytc-1a* and *cytc-1b*) plants were grown as in (f) and treated with glucose in the presence or absence of the inhibitors. The results were compared using Sidak's multiple comparisons tests ($n > 15$, $P < 0.05$), and different letters indicate significant differences.

an aliquot of RNA (1.5 μ g) using an oligo(dT)₁₈ primer and reverse transcriptase (Thermo Fisher). qPCR was performed on an aliquot of the cDNA using specific primers for the gene of interest (Supporting Information Table S1) and SYBR Green detection in a Bio-Rad CFX96 apparatus. Ct values were normalized using values for the *ACT2* actin gene (Charrier *et al.*, 2002). Results are expressed as the mean (\pm SEM) of three biological replicates.

Western blot analysis

For western blot analysis, 50 mg of fresh tissue was used to extract total soluble proteins. The samples were collected in Eppendorf tubes and immediately frozen in liquid nitrogen. Subsequently, the tissue was disaggregated, and the proteins were extracted using 75 μ l of 2 \times Laemmli buffer supplemented with 1 \times phosphatase inhibitor (PhosSTOPTM; Roche), protease inhibitor (cOmpleteTM; Roche), and 0.2 mM phenylmethylsulfonyl fluoride (PMSF). Proteins were denatured at 95°C for 5 min and then centrifuged at 12 000 *g* for 10 min. Subsequently, 10 μ l of the supernatant was separated on a 10% SDS-PAGE gel and transferred to a polyvinylidene difluoride (PVDF) membrane. The PVDF membrane was then blocked using a 5% milk solution. The primary antibodies anti-S6K (1:1000, S6K1/2, #AS121855; Agrisera), anti-P-S6K (1:1500, S6K1/2-P, #AS132664; Agrisera), anti-Actin (1:10 000, ACT, #AS132640; Agrisera), anti-GFP (1:5000, #AS152987; Agrisera), anti-CYTc (1:2000, #AS08343A; Agrisera), and anti-AOX1/2 (1:3000, #AS04054; Agrisera) were used and detected using HRP-conjugated anti-rabbit IgG (1:50 000, A16110; Thermo Fisher Scientific, Waltham, MA, USA). The primary antibody anti-HA (1:10 000, 11867423001; Roche) was detected using HRP-conjugated anti-rat IgG (1:20 000, #AS101187; Agrisera). The incubation time for blocking and primary and secondary antibodies was 1 h. Antibodies and milk were diluted in 1 \times Tris Buffered Saline containing 0.1% Tween 20.

S6K immunopurification

For immunopurification of S6K, 350 mg of fresh tissue was collected in Eppendorf tubes and immediately frozen in liquid nitrogen. Subsequently, the tissue was disaggregated and incubated for 10 min with 700 μ l of protein extraction buffer (50 mM Tris-HCl pH 7.4; 150 mM NaCl; 1 mM EDTA; 5 mM DTT; 0.2% NP-40; 1 \times phosphatase inhibitor; 1 \times protease inhibitor; 0.2 mM PMSF), followed by centrifugation at 12 000 *g* for 10 min. The supernatant was saved. Protein G magnetic beads (50 μ l) were resuspended in 1 ml dilution buffer (1.1% Triton X-100; 1.2 mM EDTA; 16.7 mM Tris-HCl pH 8; 167 mM NaCl) and conjugated with 1 μ l of anti-HA antibody for 1 h at room temperature with agitation. Subsequently, the supernatant was exposed to the conjugated beads overnight at 4°C. Following this, the beads were separated from the protein extract and the bound fraction was eluted with 50 μ l 2 \times Laemmli buffer followed by incubation at 95°C for 5 min. The mixture was centrifuged at 12 000 *g* for 5 min, and an aliquot was saved for western blot analysis.

Statistical analysis

Data were analyzed using one-way and two-way ANOVA tests (Tukey's or Sidak's *post hoc* test, $P < 0.05$). Comparisons between two samples were performed by Student's unpaired *t*-tests ($P < 0.05$).

Results

Plants with decreased CYTc levels have shorter roots, reduced growth in the presence of sugars, and altered energy metabolism

Previous reports showed that *cytc* double mutant plants with lower CYTc levels (*cytc-1b2a* and *cytc-1b2b*) exhibited delayed

germination and developmental growth transitions (Racca *et al.*, 2018, 2022). Since effects on postgerminative growth were mainly attributed to the activity of *CYTc-1*, one of the two genes encoding CYTc in *Arabidopsis thaliana*, we analyzed the phenotypic characteristics of *cytc-1* single mutant plants (*cytc-1a* and *cytc-1b*), previously described in Welchen *et al.* (2012). While the *cytc-1a* mutant is fully knock-out, *cytc-1b* has strongly reduced *CYTc-1* transcript levels due to a T-DNA insertion located 25-bp downstream of the stop codon. Both mutations cause a significant decrease in CYTc protein levels (Fig. S1). We observed that *cytc-1* mutant seedlings exhibited shorter roots than wild-type (WT) plants when grown for 6 d in a ½MS medium (Fig. 1a). Furthermore, we analyzed the root growth response to the presence of sucrose in the growth medium. Although *cytc-1* plants could respond to sucrose, this response did not allow mutants to reach the growth shown by WT plants (Fig. 1a).

We previously demonstrated that cultured cells of the *cytc* double mutant *cytc-1b2a* showed altered biogenesis and stability of respiratory Complexes III and IV. Additionally, they exhibited impaired mitochondrial respiratory activity that relied on the CYTc oxidase (COX) ATP-producing pathway (Welchen *et al.*, 2012). Here, we observed that, under the analyzed experimental conditions, root cells of single *cytc-1a* and *cytc-1b* mutant seedlings exhibited reduced staining with the cell-permeant fluorescent dye TMRM (Fig. 1b,c), which accumulates in active mitochondria depending on their membrane potential (Schwarzländer *et al.*, 2012), but not with the mitochondrial marker MitoTracker Green (Fig. 1b,d) that stains mitochondria irrespective of their membrane potential (Pendergrass *et al.*, 2004), used as a control of total mitochondrial mass. This result indicates that a deficiency in *CYTc-1* affects the energy status of root mitochondria without affecting the number of mitochondria. To further analyze this, we evaluated the ATP content in seedlings grown in MS liquid medium before and after adding sucrose for 3 h. We observed a lower ATP content in *cytc-1* mutant plants, which showed only a minor increase when plants were incubated in an energy-supplying source such as sucrose (Fig. 1e).

As an additional approach, we analyzed the effect of glucose added to seedlings grown for 3.5 d in ½MS liquid medium in a LD diurnal cycle followed by an extended night (16 h in darkness) for nutrient depletion, according to Li *et al.* (2017) and Xiong *et al.* (2013) with some modifications. Similar results (i.e. defective root growth both in the absence and presence of glucose) were observed in this case (Fig. 1f,g). Then, we tested the effect of adding the Complex III inhibitor AMA or the uncoupler agent 2,4-dinitrophenol (DNP) on the growth of roots from WT, *cytc-1a*, and *cytc-1b* mutant plants. As expected, these treatments inhibited the effect of glucose on root growth, but mutant seedlings showed a reduced sensitivity to both compounds (Fig. 1h,i). Given the TMRM and ATP results, this is probably related to mutant seedlings already showing a defect in mitochondrial energy metabolism without inhibitors.

Since a block in the CYTc-dependent respiratory pathway may cause the elicitation of an MRR response (Ng *et al.*, 2014), we evaluated the expression of the AOX and other components

of the MRR signaling pathway under the growth conditions analyzed. We observed no significant differences in expression levels, except for a decrease in *AOX1a*, which did not translate into lower AOX protein levels in CYTc-deficient plants compared with WT plants (Fig. S2a,b). Overall, the results suggest that the root growth defect in *cytc-1* mutant plants is most likely caused by altered mitochondrial function and metabolic or energetic changes that are not related to the activation of the canonical MRR.

Plants deficient in CYTc-1 exhibit changes in their free amino acid composition and display increased constitutive autophagy

We further investigated the impact of defective mitochondrial activity on the levels of plant metabolites. No significant differences in starch and soluble sugar content were observed between WT and mutant plants grown in ½MS under LD photoperiod for 5 d (Fig. S3). This result implies that the reduced growth of *cytc-1* mutant plants is not due to a lower carbon reserve content, which agrees with the fact that the exogenous addition of sugars did not recover growth to WT levels (Fig. 1a,f,g). In addition, the total free amino acid content was significantly increased in *cytc-1a* and *cytc-1b* mutant seedlings relative to WT plants (Fig. 2a). This result prompted us to analyze changes in individual amino acids. We observed a generalized increase in several amino acids in *cytc-1* mutant plants (Fig. 2b), suggesting the existence of a general alteration in amino acid metabolism.

Free amino acids increase under carbon starvation conditions since they serve as an alternative carbon source. Carbon starvation leads to the induction of autophagy, a finely tuned process that helps cells to maintain their homeostasis through the degradation and recycling of various cellular components. Therefore, we analyzed the autophagy process in CYTc-deficient plants. First, we performed staining with the dye LysoTracker Green, which marks autophagosomes that accumulate as fluorescent structures in acidic compartments (Bassham, 2015). The analysis was made in the roots of 5-d-old WT and *cytc-1* mutant plants grown vertically in ½MS with 1% (w/v) agar plates. We observed that *cytc-1* mutant plants show an increased number of structures that accumulate the dye, identified as green dots distributed in the cytoplasm of cells when viewed through confocal microscopy images, relative to WT plants (Fig. S4a,b). Similar results were observed in *cytc-1b2a* and *cytc-1b2b* double mutants (Fig. S4c,d).

Since LysoTracker Green also accumulates in acidic compartments not related to autophagosomes, we also evaluated autophagy using the 35S::GFP-ATG8a reporter line (Thompson *et al.*, 2005). Autophagy-related 8 (ATG8) is a central component of the autophagy machinery, and this tool helps to measure the dynamic flux through the entire pathway leading to degradation and nutrient reutilization (Liu & Bassham, 2010). Vacuolar degradation of GFP-ATG8 after delivery by the autophagosomes releases free GFP, and comparing the ratio of free GFP to GFP-ATG8 gives a measure of the activity of the autophagy pathway (Thompson *et al.*, 2005). Using an anti-

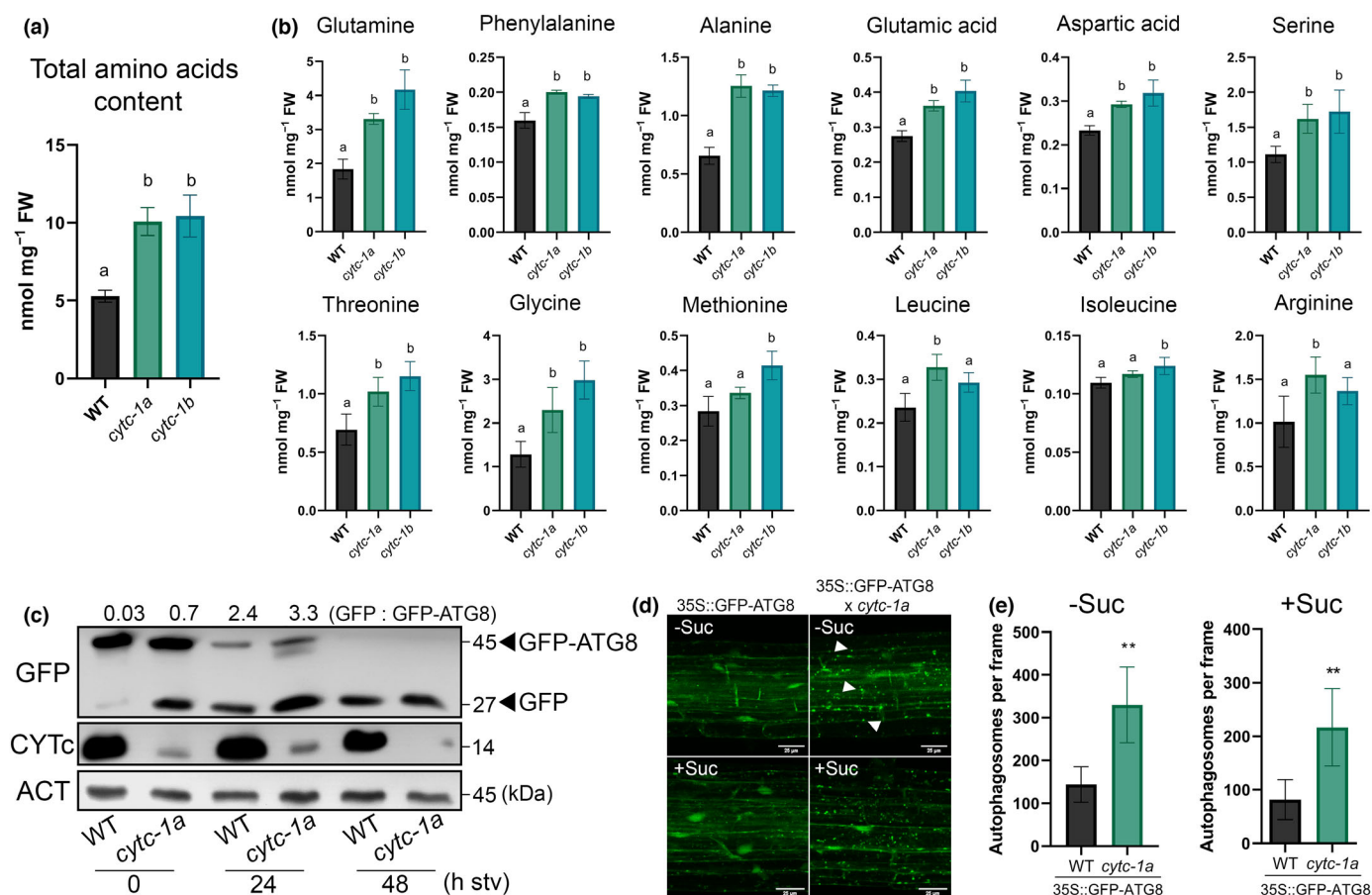


Fig. 2 *cytc-1* mutants exhibit changes in their amino acid profiles and display increased levels of autophagy under normal growth conditions. (a) Total free amino acid content (nmol mg⁻¹ FW) was determined in wild-type (WT), *cytc-1a*, and *cytc-1b* seedlings grown for 5 d in vertical plates with ½-strength Murashige & Skoog (½MS) medium containing 1% (w/v) agar and 1% (w/v) sucrose in a long-day (LD) diurnal cycle. Bars represent mean (±SD). Different letters indicate significant differences based on Tukey's test (three biological replicates, $P < 0.05$). (b) Individual amino acids profile determined by high-performance liquid chromatography (HPLC) on the plant extracts evaluated in (a). Bars represent mean (±SD). Different letters indicate significant differences based on Tukey's test (three biological replicates, $P < 0.05$). (c) Immunoblot analysis showing the dynamics of autophagy by quantifying the GFP : GFP-ATG8 ratio, using an anti-GFP antibody (#AS152987; Agrisera) in total protein extracts made from WT and *cytc-1a* mutant plants in the 35S::GFP-ATG8a background (35S::GFP-ATG8 in the figures for simplicity). An anti-CYTc antibody (#AS08343A; Agrisera) was used to corroborate the identity of the lines used. An anti-Actin antibody (#AS132640; Agrisera) was used as a loading control in the same membrane. Seedlings were grown for 5 d in vertical plates with ½MS medium containing 1% (w/v) agar and 1% (w/v) sucrose in a LD diurnal cycle and then exposed to darkness for 24 h and 48 h (h stv, h after transfer to darkness). Numbers above the image correspond to the ratio GFP/GFP-ATG8 and those on the side indicate the molecular weight (kDa) of each protein. (d) Representative images acquired by confocal microscopy from 5-d-old root cells of WT and *cytc-1a* plants in the 35S::GFP-ATG8a background. Plants were grown for 5 d in vertical plates with MS medium containing 1% (w/v) agar (-Suc, upper panels) or similar plates supplemented with 1% (w/v) sucrose (+Suc, lower panels) in a LD diurnal cycle. Bars, 25 µm. (e) Quantification of the number of autophagosomes per frame. Statistical analysis is based on Student's *t*-tests ($P < 0.05$, $n > 10$ roots).

GFP antibody, we observed a significant increase in the free GFP to GFP-ATG8 ratio in *cytc-1a* mutant plants compared with WT plants under normal growth conditions (Fig. 2c). An increase in GFP : GFP-ATG8 ratio was observed in both genotypes after prolonged darkness. This suggests that the dynamics of protein degradation through the autophagy pathway are basally higher in the *cytc-1a* mutant background. GFP-ATG8 also marks the presence of autophagosomes from the early stages of phagophore expansion to the final vacuolar degradation reactions. This can be used to quantify the amount of these structures by confocal microscopy (Thompson *et al.*, 2005). Once

again, our observations showed an increased number of GFP-labeled autophagosomes in the roots of the *cytc-1a* mutant (Fig. 2d,e). This result indicates that the increased staining observed with LysoTracker Green is indeed due to an increase in autophagic activity. Interestingly, the difference with WT plants remained even when the seedlings were grown with 1% sucrose (+Suc) on the MS agar plates (Fig. 2d,e). In conclusion, a deficiency in *CYTc-1* can trigger the process of autophagy even if these plants do not seem to undergo carbon starvation. This is supported by the fact that increased autophagy was also observed after adding exogenous sugar.

The autophagy process becomes relevant in *cytc-1* mutant plants during carbon starvation stress

Given the phenotypic and metabolic characteristics described for *cytc-1* mutant plants, we conducted a study to assess the impact of blocking autophagy in these plants. Our approach involved the use of *atg5-1* and *atg7-2* single mutants, both in genes coding for essential autophagy factors involved in plant nutrient recycling (Thompson *et al.*, 2005), and crossing them with *cytc-1a* and *cytc-1b* mutant lines. We analyzed the number of autophagosome-like structures present in the roots of these double mutant plants by staining with LysoTracker Green and visualization by confocal microscopy (Fig. S5). Our findings showed that the number of these structures in the double *atg* × *cytc-1* mutant lines decreased to levels comparable to those of the *atg5-1* and *atg7-2* mutant lines (Fig. 3a,b), indicating that these structures indeed correspond to autophagosomes. Furthermore, this reduction was associated with a decrease in total free amino acid content to WT levels (Fig. 3c,d). When analyzing the phenotype of the *atg5-1* × *cytc-1a* and *atg7-2* × *cytc-1b* double mutants, we observed that blocking autophagy does not affect the root growth of WT plants or plants with lower CYTc levels, either in the presence or absence of 1% sucrose (Fig. 3e,f). In addition, the rosette area of the *atg5-1* × *cytc-1a* and *atg7-2* × *cytc-1b* double mutants at the adult vegetative stage grown in soil under LD photoperiod are also comparable to that of plants with decreased CYTc-1 levels (Fig. 3g). The findings suggest that increased autophagy is not responsible for the defective growth of plants with lower CYTc levels. Furthermore, the alternative hypothesis that these plants may use autophagy as a source of carbon skeletons for growth under normal conditions does not seem valid either.

Autophagy is increased under nutrient-limiting conditions to help replenish internal supplies during senescence or stress. Therefore, to analyze whether blocking autophagy affected the behavior of *CYTc-1* deficient plants, we evaluated the phenotypic characteristics of *atg5-1* × *cytc-1a* and *atg7-2* × *cytc-1b* double mutants under carbon starvation elicited by dark-induced senescence (Fig. 3h). We accomplished this by exposing 7-d-old plants maintained in ½MS with 20 mM sucrose liquid medium to darkness and sucrose starvation for 7 more days. At the end of the experiment, total chlorophyll content was evaluated in plants grown under normal conditions (control) and in plants subjected to carbon starvation (-C). Chlorophyll content was comparable among all lines when plants were grown under optimal conditions (Fig. 3i, left panel, control). However, the *cytc-1* mutants retained a higher level of chlorophyll than WT plants after prolonged darkness (Fig. 3i, right panel, -C). By contrast, when the autophagy process was blocked, as seen in the *atg5-1* and *atg7-2* mutant backgrounds, chlorophyll content dropped significantly to levels comparable to those of the respective autophagy mutant parents (Fig. 3h,i).

Our result indicates that *cytc-1* mutants are more resistant to nutritional stress, similar to observations made with plants with a triggered starvation signal (Mair *et al.*, 2015). This evidence is also consistent with plants with lower CYTc levels showing a

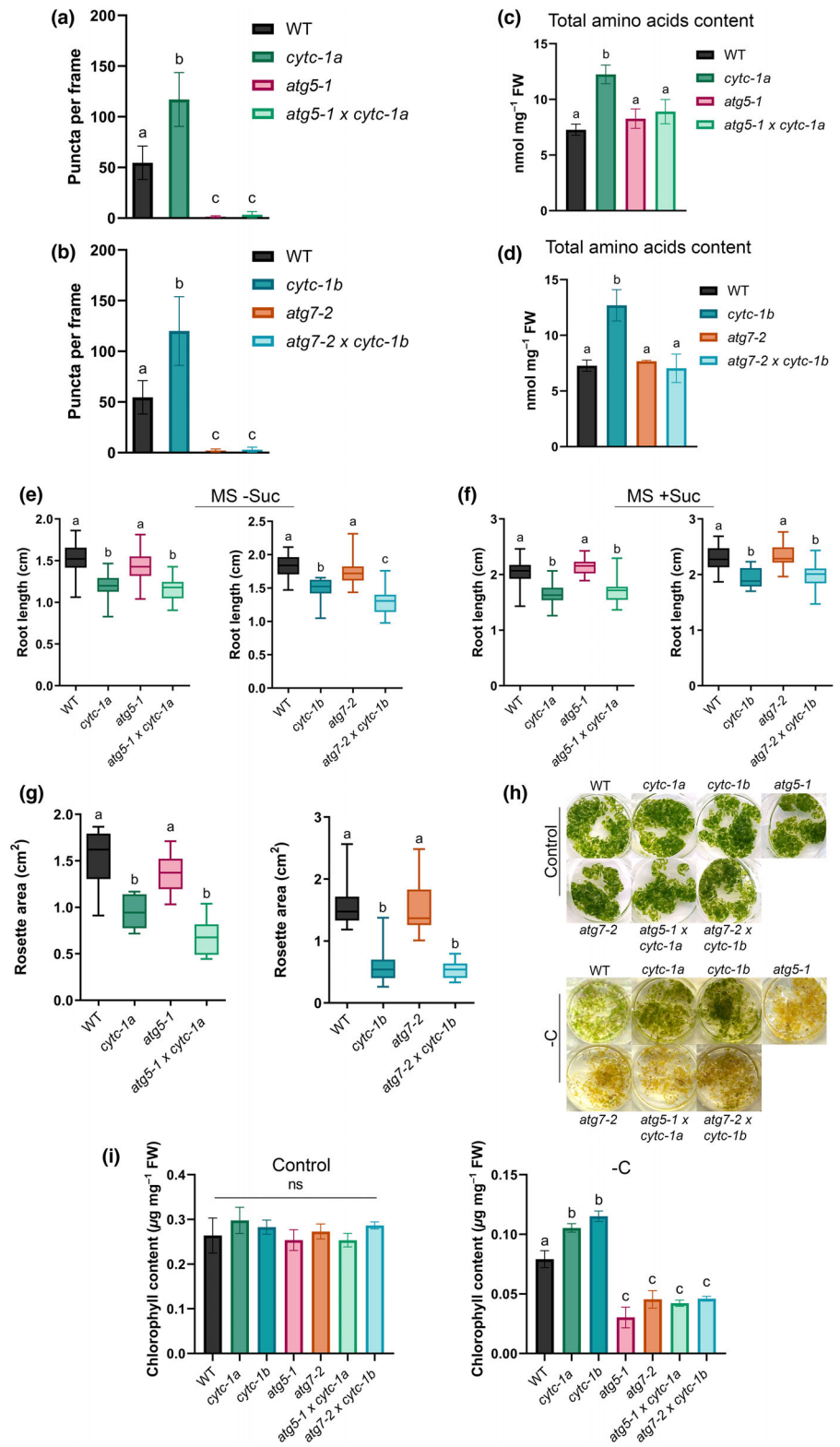
delayed entry into the natural senescence stage (Welchen *et al.*, 2012). Therefore, we propose that *cytc-1* mutant plants use autophagy-derived nutrients to cope with the increased nutritional stress related to nutrient deprivation. However, the autophagy pathway does not play a particular role in growth under normal LD conditions.

The *cytc-1* deficient plants have reduced activity of the TOR pathway

We found that several characteristics of plants with lower CYTc levels, like defective growth, increased autophagy, and increased free amino acid content, are similar to those of plants defective in TOR-pathway components (Salem *et al.*, 2017). TOR is a conserved protein kinase that regulates crucial cellular processes in eukaryotes, including mRNA translation, cell division, chloroplast function, anabolic metabolism, hormone responses, and autophagy, transducing metabolic signals for growth. Thus, we inquired about a possible connection between CYTc levels, the CYTc-dependent mitochondrial respiratory pathway, and the TOR pathway. Related to this, we also noticed that plants with low CYTc levels show hyposensitivity to the addition of AZD-8055 (AZD), a selective ATP-competitive inhibitor of TOR complex activity (Montané & Menand, 2013; Fig. 4a). AZD sensitivity is a criterion previously utilized in genetic screens to identify players in the TOR pathway (Schaufelberger *et al.*, 2019). Accordingly, we directly analyzed the activity of the TOR pathway by measuring the activation status of the ribosomal protein S6K using antibodies against the phosphorylated variant of this protein (P-S6K; Mahfouz *et al.*, 2006). This strategy is widely used to monitor changes in TOR-pathway activity (Xiong *et al.*, 2013). Our results showed that the levels of P-S6K are lower in the *cytc-1* mutant background compared with WT plants, as observed in 4-d-old seedlings grown in ½MS medium and treated with 20 mM sucrose for 3 h to activate the TOR pathway (Fig. 4b). Notably, total S6K levels seemed also lower in the *cytc-1* mutant background than in WT plants (Fig. 4b). To further evaluate this, we performed crosses between the *cytc-1a* line and a 35S::S6K-HA reporter line (Fig. S6a; Henriques *et al.*, 2013). We used antibodies against hemagglutinin (HA) to monitor total S6K levels. Lower S6K-HA total levels were observed in the *cytc-1a* mutant background, with a marked decrease in the levels of S6K phosphorylation (Fig. 4c). We also measured S6K transcript levels in WT, *cytc-1a*, and *cytc-1b* backgrounds to determine whether the observed changes in total S6K levels were due to different transcriptional activities of the respective genes. No significant differences in transcript levels were observed (Fig. S6b), suggesting that CYTc deficiency post-transcriptionally affects S6K protein levels at this developmental stage. This observation is also indicated by the fact that lower S6K-HA levels are present in the *cytc-1* mutant background, even with the *CaMV35S* promoter driving its expression.

Additionally, we analyzed expression levels of S6K and other members of the TOR pathway in different tissues and developmental stages of *CYTc-1* deficient plants (Fig. S6b–d). At the transcriptional level, we only observed a slight decrease in

Fig. 3 Autophagy is responsible for the increased amino acid content and becomes relevant in *cytc-1* mutant plants during carbon starvation. (a, b) Quantification of the number of puncta stained with LysoTracker Green per frame of 5-d-old root cells. Plants were grown in vertical plates with MS medium containing 1% (w/v) agar and 1% (w/v) sucrose in long-day (LD) diurnal cycle and stained with 1 μ M LysoTracker Green dye (Invitrogen). Different letters indicate significant differences based on Tukey's test ($n > 8$ roots, $P < 0.05$). The genotypes analyzed were wild-type (WT), *cytc-1* mutants (*cytc-1a* and *cytc-1b*), *atg* mutants (*atg5-1* and *atg7-2*), and the respective double mutant lines (*atg5-1* \times *cytc-1a* and *atg7-2* \times *cytc-1b*). (c, d) Total free amino acid content (nmol mg^{-1} FW) was determined in the same genotypes mentioned in (a, b). Different letters indicate significant differences based on Tukey's test (four biological replicates, $P < 0.05$). (e, f) Root length (cm) measured in 6-d-old seedlings grown in vertical plates with $\frac{1}{2}$ -strength Murashige & Skoog medium containing 1% (w/v) agar either in the absence (e) or presence (f) of 1% (w/v) sucrose (Suc) in a LD diurnal cycle. Different letters indicate significant differences based on Tukey's test ($n > 10$, $P < 0.05$). (g) Quantification of rosette area (cm^2) of WT, *cytc-1* mutants (*cytc-1a* and *cytc-1b*), *atg* mutants (*atg5-1* and *atg7-2*), and the respective double mutant lines (*atg5-1* \times *cytc-1a* and *atg7-2* \times *cytc-1b*) of plants grown on soil during 17 d in LD diurnal cycle. The boxplot represents the median and the upper and lower quartile. Whiskers indicate variation in the data. Different letters indicate significant differences based on Tukey's test ($n > 8$, $P < 0.05$). (h) Representative images of seedlings from a carbon starvation assay. Seedlings of the genotypes mentioned in (a, b) were grown for 3.5 d in MS liquid medium followed by an extended night for nutrient depletion (16 h darkness) and then treated with 20 mM sucrose for 3 d to induce growth. After that, half of the plants were kept on sucrose for 7 d to constitute the 'control condition' (top panel), and the rest was placed in darkness without sucrose for the same time to induce carbon starvation condition ('-C', bottom panel). (i) Effect of carbon starvation on the chlorophyll content ($\mu\text{g} \text{mg}^{-1}$ FW) of plants with decreased autophagy and/or cytochrome c (CYTc) levels. The left panel corresponds to the control conditions and the right panel refers to the carbon starvation condition ('-C'). Bars represent the mean (\pm SD). Different letters indicate significant differences based on Tukey's test (five biological replicates, $P < 0.05$), ns, not significant.



transcript levels for *S6K1* and *LST8* (Lethal with SEC13 protein 8) in rosette leaves of *cytc-1* mutant plants (Fig. S6c,d). On the other hand, S6K protein levels were markedly decreased in *cytc-1* mutant plants at different developmental stages, both in the apical meristem (Fig. 4e) and in rosette leaves of adult plants grown

under LD photoperiod (Fig. 4f). These results suggest that CYTc deficiency affects S6K protein levels in various tissues of the plants and across different developmental stages.

We considered whether S6K might be more unstable in cells with altered mitochondrial activity due to decreased CYTc.

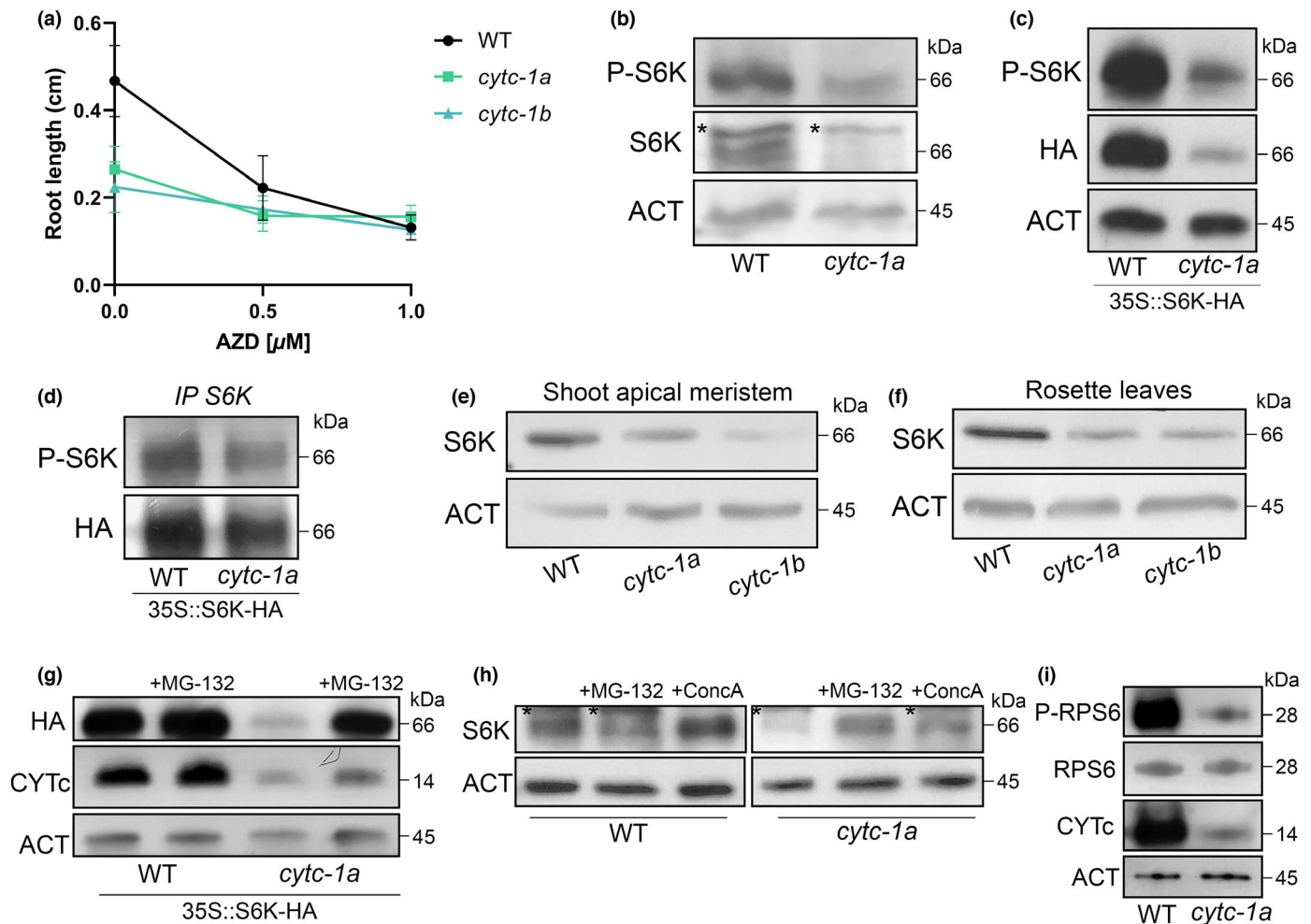


Fig. 4 Target of rapamycin (TOR) pathway is altered in *cytc-1* mutants. (a) Sensitivity to TOR-pathway inhibition was analyzed as the reduction in root length caused by AZD-8055 (AZD) in wild-type (WT), *cytc-1a*, and *cytc-1b* seedlings grown in $\frac{1}{2}$ -strength Murashige & Skoog liquid medium for 3.5 d followed by an extended night for nutrient depletion (16 h darkness) and supplemented with sucrose (20 mM) and different concentrations of AZD in the culture medium for two additional days. Each individual point represents the mean (\pm SD). (b) Western blot analysis of S6 kinase (S6K) protein levels and its phosphorylated form (P-S6K) in WT and *cytc-1a* seedlings. Seedlings were grown for 3.5 d in MS liquid medium followed by an extended night for nutrient depletion (16 h darkness) and then treated with 20 mM sucrose for 3 h. The analysis was performed in total protein extracts with specific antibodies against S6K (#AS121855; Agrisera) and P-S6K (#AS132664; Agrisera). Stars represent unspecific bands. (c) Western blot analysis to evaluate S6K-HA and P-S6K levels in WT and *cytc-1a* seedlings in the 35S::S6K-HA background. Anti-HA antibodies (Roche 11867423001) were used to measure S6K-HA levels and anti-P-S6K was used to evaluate the phosphorylated fraction. (d) Western blot analysis of S6K-HA and P-S6K levels after immunoprecipitation of S6K-HA from 35S::S6K-HA and 35S::S6K-HA \times *cytc-1a* lines. The immunoprecipitation was performed using HA antibody-conjugated magnetic beads from total protein extracts of seedlings grown as indicated in (b). (e, f) S6K levels were assessed in total protein extracts from WT, *cytc-1a*, and *cytc-1b* shoot apical meristem (e) and rosette leaves (f) of 15-d-old plants grown in soil under long-day (LD) conditions. (g) Evaluation of S6K-HA levels in total protein extracts made from WT and *cytc-1a* plants (both in the 35S::S6K-HA background) in response to treatment with the proteasome inhibitor MG-132. Seedlings were grown as indicated in (b), and MG-132 (20 μM) was added to a group of plants to inhibit proteasomal protein degradation. Anti-HA was used to measure S6K-HA levels and anti-CYTc antibody was used to corroborate the identity of the lines used. (h) Western blot analysis for evaluating endogenous S6K levels in response to MG-132 and Concanamycin A (ConcA; 1 μM) for autophagy inhibition. Seedlings were grown as indicated in (b). Stars represent unspecific bands. (i) Western blot analysis of RPS6 (#AS194292; Agrisera) and its Ser240 phosphorylated isoform (P-RPS6, #AS194302; Agrisera) levels, measured in total protein extracts from WT and *cytc-1a* seedlings grown as indicated in (b). An anti-CYTc antibody was used to corroborate the identity of the lines used and anti-Actin (ACT) was used as a loading control in all these experiments. The number on each blot represents the molecular weight of each protein.

Therefore, we analyzed the effect of CYTc deficiency on S6K protein. We observed that adding the proteasome inhibitor MG-132 caused a more significant increase in S6K levels in *cytc-1a* mutant plants than in WT plants when either endogenous S6K or S6K-HA were analyzed (Fig. 4g,h). Furthermore, given the increased levels of basal autophagy observed in *cytc-1* mutants

(Fig. 2), we examined the effect of inhibiting the vacuolar H^+ -ATPase using Concanamycin A (ConcA), which inhibits the vacuolar degradation of proteins in autophagic bodies (Liu & Bassham, 2010; Forzani *et al.*, 2019), on S6K levels in *cytc-1* mutant plants. We observed a significant increase in total S6K protein levels, particularly in the *cytc-1a* background, after

treatment with ConA (Fig. 4h). Our findings suggest that the levels of S6K are decreased in the *cytc-1* mutant plants due, at least in part, to a more significant degradation through the 26S proteasome and the autophagy process. However, it remains to be determined whether, in addition to the processes evaluated, there is a specific and differential regulation of S6K translation in the background of *cytc-1* mutants.

To assess whether the proportion of P-S6K relative to total S6K levels is affected in the mutant, we performed an immunoprecipitation (IP) assay using anti-HA beads to isolate S6K-HA protein. We observed that the level of S6K phosphorylation (P-S6K) is only slightly reduced in the *cytc-1a* mutant background compared with the 35S::S6K-HA reporter line in the WT background after equalizing S6K-HA protein levels (Fig. 4d). This result indicates that a deficiency in CYTc affects the amount of P-S6K primarily through changes in total S6K levels. Another robust readout to assess activation of the TOR pathway is the level of the phosphorylated variant of the 40S Ribosomal Protein S6 (P-RPS6), a direct target of S6K. Thus, lower activation of the TOR pathway affects P-RPS6 levels through changes in the activity of S6K (Dobrenel *et al.*, 2016). When analyzing the same total protein extracts used to measure S6K and P-S6K levels (Fig. 4b), we observed that total RPS6 protein levels were comparable between WT and *cytc-1a* mutant plants (Fig. 4i). However, a much lower signal was observed in *cytc-1a* mutant plants when using the antibody against the phosphorylated variant (P-RPS6), confirming a lower activation of the TOR pathway in CYTc-1 deficient plants (Fig. 4i). A decrease in P-RPS6 levels was also observed in the double *cytc-1b2a* mutant background (Fig. S7). These results indicate that the observed changes in S6K levels and phosphorylation state affect downstream processes related to S6K activity. Overall, we conclude that a decrease in CYTc levels modifies the activity of the TOR signaling pathway, affecting the stability and/or the phosphorylation status of S6K and downstream components.

Increased TOR expression reverses the detrimental effects of CYTc deficiency on growth and metabolism

Our previous research suggests that CYTc levels play a crucial role in plant growth, as its deficiency and overexpression significantly affect plant growth rate (Welchen *et al.*, 2012; Racca *et al.*, 2018, 2022). To examine a possible connection between CYTc and the TOR pathway, we analyzed CYTc protein levels in plants affected by different components of this pathway. We observed that *raptor1b*, *rps6b*, and *lst8-1* mutants show increased CYTc protein levels (Figs S8a, S9 showing the raw images of the western blot analyses), in agreement with a global proteomic study performed by Montes *et al.* (2022), showing an increment in CYTc-1 (At1g22840) and CYTc-2 (At4g10040) levels in the background of *raptor1b* mutant plants. In addition to this, we conducted an experiment to overexpress CYTc in the background of the TOR-pathway mutants *raptor1b* and *rps6b* (Salem *et al.*, 2017; Chen *et al.*, 2018). We found that increased CYTc levels did not alter the mutant phenotype, characterized by reduced root length measured on 6-d-old seedlings grown on vertical

plates and reduced rosette size of adult plants grown in soil under LD photoperiod (Fig. S8b–d), suggesting that the effect of CYTc on growth requires an active TOR pathway.

Inversely, we performed crosses between a *cytc-1* mutant line and a GFP-TOR overexpression line (35S::GFP-TOR; Schepetilnikov *et al.*, 2017; Fig. 5a) to study to what extent the observed decrease in TOR-pathway activity is responsible for the reduced growth and other characteristics of *CYTc-1*-deficient plants. Interestingly, we found that the 35S::GFP-TOR × *cytc-1a* line showed similar root growth characteristics to those of WT plants, even though overexpression of GFP-TOR did not seem to enhance growth in a WT background under the same condition (Fig. 5b top panel,c). Similar restoration of growth parameters, comparable to those of WT plants, was observed at vegetative stage, evaluated by the analysis of the rosette area at different times (Fig. 5b bottom panel,d), and also at flowering time (Fig. 5e).

Next, we characterized the 35S::GFP-TOR × *cytc-1a* line at the molecular level to inspect whether GFP-TOR expression also restores other parameters affected in *cytc-1* mutant plants. We observed that the activity of the TOR pathway, as measured by P-S6K and P-RPS6 levels, was significantly increased in the 35S::GFP-TOR × *cytc-1a* line compared with the levels observed in the *cytc-1a* mutant (Fig. 5f). Interestingly, S6K protein levels were also restored (Fig. 5f), indicating that the previously demonstrated effect of CYTc deficiency on S6K stability (Fig. 4g,h) is also related to a decreased TOR-pathway activity.

Besides regulating growth, the TOR kinase inhibits autophagy by phosphorylating the autophagy-related protein ATG13a (Van Leene *et al.*, 2019). Therefore, according to the increased basal autophagy detected in *cytc-1* mutants (Fig. 2c–e), we evaluated this process in the *cytc-1a* plants with restored TOR-pathway activity. The number of structures labeled with LysoTracker Green in 35S::GFP-TOR × *cytc-1a* plants was similar to that of WT plants and much lower than that observed in *cytc-1a* mutant plants (Fig. 6a,b), suggesting that expression of GFP-TOR causes a decrease in autophagic activity in the mutant. Coincident with the reduced levels of autophagy, the content of total free amino acids returned to levels comparable to those of WT plants (Fig. 6c) due to the normalization of individual amino acid profiles (Fig. S10). These results indicate that the constitutive activation of the autophagy pathway observed in *CYTc-1* deficient plants results from the lower activity of the TOR pathway observed in these plants under normal growth conditions.

Finally, regarding the connection between mitochondrial activity and the TOR kinase pathway, we evaluated the mitochondrial membrane potential in 35S::GFP-TOR × *cytc-1a* plants using TMRM staining. Mitochondrial membrane potential remained low and comparable to that of *cytc-1a* mutant plants after expressing GFP-TOR (Fig. 6d,e), and the number of mitochondria, revealed by MitoTracker Green staining, remained unchanged in this line compared with WT, 35S::GFP-TOR, and *cytc-1a* parental plants (Fig. 6f,g). Additionally, upon evaluating the ATP content in *CYTc-1* deficient plants with elevated levels of GFP-TOR, we found that it was significantly lower in 35S::GFP-TOR × *cytc-1a* plants compared with that measured in *cytc-1a*

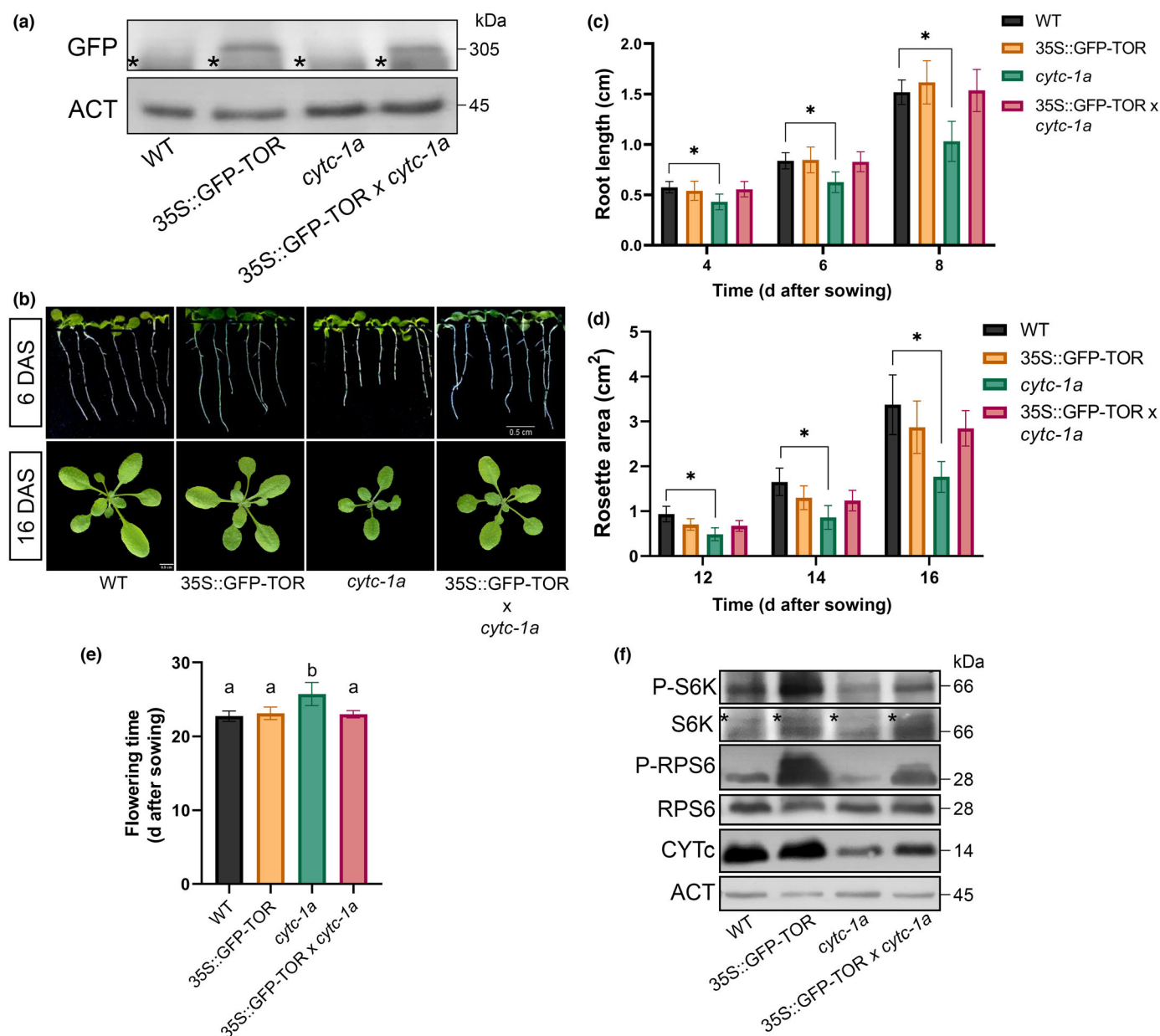


Fig. 5 Increasing target of rapamycin (TOR)-pathway activity recovers growth in *cytc-1* mutants. (a) Western blot analysis made on total protein extracts using antibodies against GFP in transgenic 35S::GFP-TOR lines in wild-type (WT) and *cytc-1a* backgrounds. Seedlings were grown as specified in Fig. 4(b). An anti-Actin antibody was used as a loading control. Stars represent unspecific bands. The numbers indicate the molecular weight (kDa) of each protein. (b) Representative images of WT, 35S::GFP-TOR, *cytc-1a*, and 35S::GFP-TOR x *cytc-1a* 6-d-old seedlings (upper panel) and rosettes of 16-d-old adult plants (lower panel). Seedlings were grown in vertical plates with 1/2-strength Murashige & Skoog medium supplemented with 1% (w/v) agar under long-day (LD) diurnal cycle. Adult plants were grown in soil under LD photoperiod. Bars, 0.5 cm. (c) Root length (cm) of seedlings mentioned in (b). The growth was recorded 4, 6, and 8 d after sowing (DAS). Asterisks indicate significant differences with WT plants, based on Student's *t*-tests ($P < 0.05$, $n > 12$). (d) Rosette area (cm²) of plant lines mentioned in (b). Data were recorded 12, 14, and 16 DAS. Asterisks indicate significant differences with WT plants, based on Student's *t*-tests ($P < 0.05$, $n > 9$). (e) Flowering time (DAS) was registered for the genotypes mentioned above. Bars represent the mean (\pm SD). Different letters indicate significant differences based on Tukey's test ($n > 9$ plants, $P < 0.05$). (f) Western blot analysis made on total protein extracts using antibodies against cytochrome *c* (CYTc), RPS6, P-RPS6, S6 kinase (S6K), and P-S6K in transgenic 35S::GFP-TOR lines in WT and *cytc-1a* backgrounds. Seedlings were grown as specified in Fig. 4(b). An anti-Actin antibody was used as a loading control. Stars represent unspecific bands. The numbers indicate the molecular weight (kDa) of each protein.

mutant plants (Fig. 6h). This outcome may be attributed to the fact that by normalizing TOR activity levels, we promoted growth and inhibited autophagy in *cytc-1* mutant plants, without

normalizing mitochondrial activity. Consequently, growth optimization in *cytc-1* mutants is probably achieved at the expense of increased ATP consumption.

Discussion

Plants coordinate their growth and metabolism based on the availability of nutrients and energy provided mainly by the chloroplast photosynthetic machinery and mitochondrial OXPHOS. However, despite extensive work, issues such as how mitochondria sense energy requirements to ensure growth (anterograde signals) and how they communicate their status to the rest of the cell for proper coordination (retrograde signals) are not fully solved (De Clercq *et al.*, 2013; Ng *et al.*, 2013, 2014; Welchen *et al.*, 2021; Welchen & Gonzalez, 2021). In this work, we aimed to understand better how the communication between mitochondria and the growth-regulatory pathway mediated by the TOR kinase complex is established, using plants with a deficiency in the mETC component CYTc (Fig. 7).

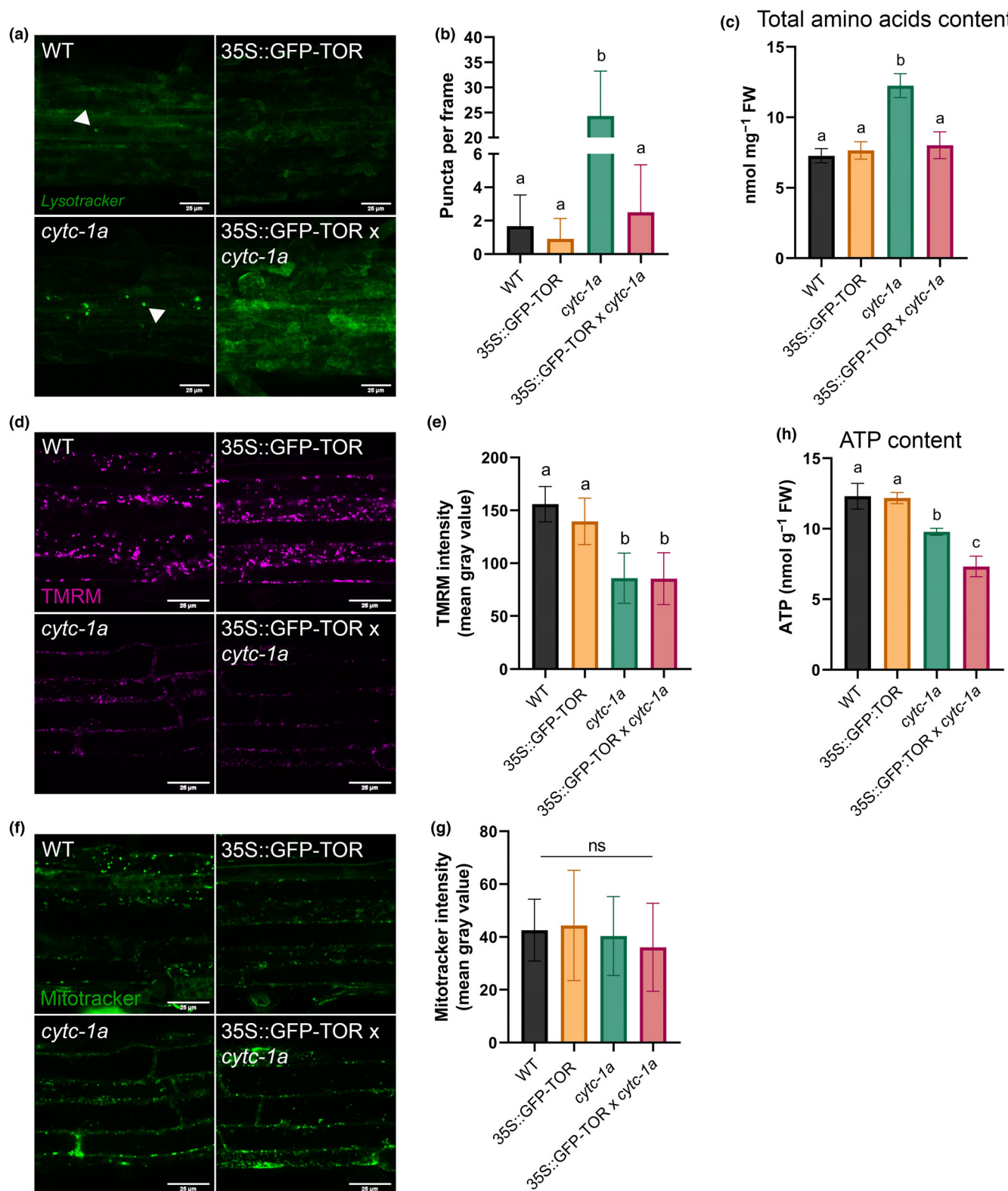
We previously reported that, while a complete CYTc deficiency is embryo lethal, double mutants in both *CYTc* genes from *Arabidopsis* (knock-down in *CYTc-1* and knock-out in *CYTc-2*) show growth defects, including delayed germination and developmental transitions, but are able to complete their life cycle and efficiently reproduce (Welchen *et al.*, 2012; Racca *et al.*, 2018, 2022). Here, we found that *cytc-1* single mutant seedlings (Fig. S1) also show stunted root growth and reduced growth rate compared with WT plants under normal conditions and after growth stimulation by sugar supplementation (Fig. 1a,f,g). This can be attributed to a constitutively reduced mitochondrial activity, as evidenced by decreased membrane potential and lower ATP content in mutant plants (Fig. 1b–e). Notably, the defects observed in *cytc-1* mutants do not affect AOX1/2 protein levels and the MRR signaling pathway (Fig. S2), which is induced after severe blockage of the CYTc-dependent respiratory chain (Ng *et al.*, 2013, 2014). This probably indicates that mild defects in CYTc-dependent respiration are transmitted to the rest of the cell independently from the canonical MRR pathway.

We also observed a notable increase in most free amino acids in *cytc-1* mutant plants, indicating significant metabolic changes associated with the energetic deficit and its consequences on plant growth (Fig. 2a,b). Our previous study demonstrated that *cytc* double mutants (*1b2a* and *1b2b*) accumulate higher starch reserves and soluble sugars in the rosette leaves of adult plants, along with an increment of specific amino acids such as Phe and the branched-chain amino acids (BCAA) Val, Leu, and Ile (Racca *et al.*, 2018). Interestingly, seedlings of the *cytc-1* single mutants did not show significant differences in starch and soluble sugar levels compared with WT (Fig. S3). Nevertheless, it seems that plants with CYTc deficiency do not use a higher proportion of carbon reserves to restore energy levels and plant growth. Instead, it is possible that *cytc-1* mutants increase their levels of free amino acids in response to a signal of carbon starvation, similar to what was previously suggested in other plants (Hildebrandt *et al.*, 2015), even if carbon reserves are normal. In this sense, *cytc-1* mutant plants exhibit increased constitutive autophagy (Figs 2c–e, S4), which in turn explains the basal increment in free amino acids content (Fig. 2a; Kacprzak & Van Aken, 2022). Autophagy is crucial in regulating plant responses to internal and environmental stimuli, maintenance and differentiation of

meristems, and responses to carbon suppression or nutrient starvation. Although autophagy is suppressed in nonstressed conditions, increased basal autophagy in *cytc-1* mutant plants is maintained even when plants are grown in the presence of an exogenous carbon source (Fig. 2d,e). These observations further suggest that a carbon starvation signal that is not directly linked to carbon availability is turned on in CYTc-deficient plants.

We considered the possibility that the induction of autophagy might cause reduced growth due to the degradation of cellular components and altered metabolism. However, growth remains stunted even when autophagy is blocked in the background of the *atg5-1* and *atg7-2* mutants (Fig. 3e–g). On the other hand, growth was not further affected after the suppression of autophagy and normalization of amino acid levels, which suggests that *cytc-1* mutants do not require free amino acids as an additional carbon source for growth under normal conditions. So far, basal autophagy induced in *cytc-1* mutant plants is essential in regulating survival when plants are exposed to starvation stress generated during prolonged growth in darkness (Fig. 3h,i). Additionally, plants with lower CYTc levels show a delayed onset of natural senescence (Welchen *et al.*, 2012). These observations support the idea that CYTc-deficient plants have an increased resistance to nutrient stress conditions, similar to that of starved plants (Mair *et al.*, 2015).

After a thorough analysis of the phenotype of *cytc-1* deficient (Figs 1–3) and double mutant plants (Welchen *et al.*, 2012; Racca *et al.*, 2018, 2022), we noticed that they share specific characteristics that have been previously reported in plants with lower levels of proteins in the TOR kinase pathway. These features included reduced growth, delayed passage to the reproductive stage and senescence (Deprost *et al.*, 2007; Salem *et al.*, 2017; Chen *et al.*, 2018), increased free amino acids content (Caldana *et al.*, 2013; Cao *et al.*, 2019; Forzani *et al.*, 2019), and increased basal autophagy (Liu & Bassham, 2010). Indeed, we found that plants with reduced CYTc levels displayed hypersensitivity to TOR inhibition (Fig. 4a), a possible indication of reduced TOR activity (Belda-Palazón *et al.*, 2022). In agreement, CYTc-deficient plants exhibited reduced activation of the TOR pathway, as evidenced by decreased P-S6K and P-RPS6 levels compared with WT plants (Fig. 4b–d,i). This reduced activation is most likely the reason behind the defective growth, increased autophagy, and increased amino acid content observed in the *cytc-1* mutant background (Figs 1–3), as suggested by the fact that these parameters are normalized to WT values after overexpressing TOR in these plants (Figs 5, 6a–c). However, parameters related to mitochondrial energy metabolism, like membrane potential and ATP levels, are not restored by TOR overexpression (Fig. 6d–g). In fact, lower ATP levels were observed in 35S::GFP-TOR × *cytc-1a* plants compared with their respective parents (Fig. 6h), indicating that the consumption of ATP fuels growth in the mutants after GFP-TOR expression. A recent study by Dai *et al.* (2022) suggested that the TOR pathway is essential for controlling physiological ATP production in plant cells. Interestingly, our observations suggest that growth optimization in the 35S::GFP-TOR × *cytc-1a* plants is achieved at the expense of increased ATP consumption from the energy

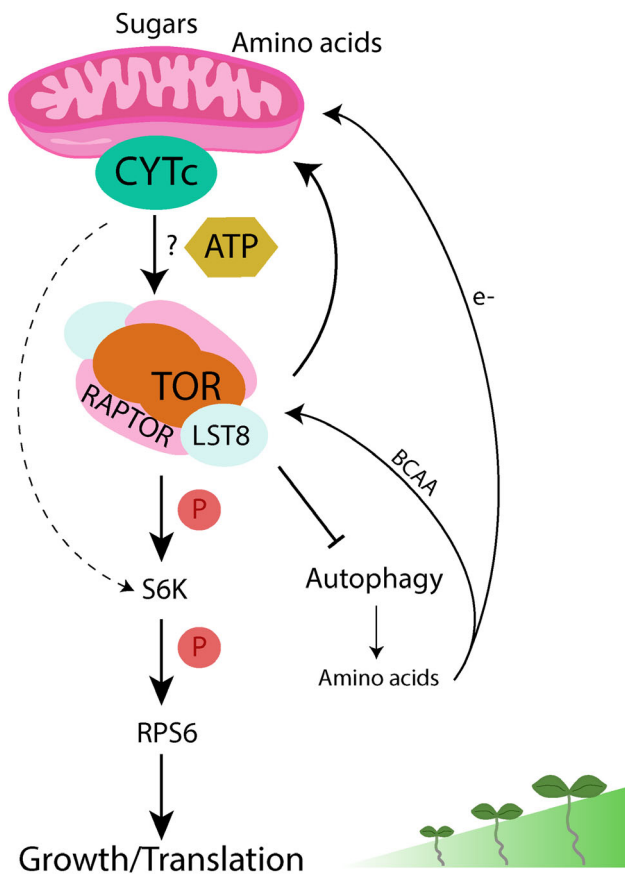


reserves (Figs 6h, 7). While the mechanism by which normalization of TOR activity restores growth has yet to be fully understood, it is clear that it is not mainly due to an increase in ATP levels. Hence, additional signals driven by the normalized TOR activity are responsible for restoring growth in plants

deficient in CYTc. The potential benefits of enhanced nitrogen uptake and utilization (Lutt & Brunkard, 2022), optimized metabolism (Ingargiola *et al.*, 2023), and hormonal pathways (Liao *et al.*, 2023) are among the possible explanations that we pursue to evaluate in future work.

Fig. 6 Autophagy and amino acid content, but not ATP, are restored to wild-type (WT) levels in 35S::GFP-TOR \times *cytc-1a* plants. (a) Representative images acquired by confocal microscopy of 5-d-old root cells of WT, *cytc-1a*, 35S::GFP-TOR, and 35S::GFP-TOR \times *cytc-1a* lines stained with 1 μ M LysoTracker Green dye. The arrows indicate structures similar to autophagosomes. Plants were grown for 5 d in vertical plates with half MS medium containing 1% (w/v) agar and 1% (w/v) sucrose in a long-day (LD) diurnal cycle. Bars, 25 μ m. (b) Quantification of the number of puncta stained with LysoTracker Green per frame corresponding to the experiment shown in (a). Bars represent mean (\pm SD). Different letters indicate significant differences based on Tukey's test ($n > 10$ roots, $P < 0.05$). (c) Total amino acid content (nmol mg^{-1} FW) was determined in WT, 35S::GFP-TOR, *cytc-1a*, and 35S::GFP-TOR \times *cytc-1a* seedlings, grown as indicated in (a). Bars represent mean (\pm SD). Different letters indicate significant differences based on Tukey's test (three biological replicates, $P < 0.05$). (d) Evaluation of mitochondrial membrane potential. Representative images were acquired from 5-d-old root cells by confocal microscopy. Plants grown as indicated in (a) were stained with 1 μ M tetramethylrhodamine methyl ester (TMRM). Bars, 25 μ m. (e) Quantification of the TMRM fluorescence intensity observed in (d). Bars represent the mean (\pm SD) of the mean gray value, analyzed per unit root area with Fiji software. Different letters indicate significant differences based on Tukey's test ($n > 10$ roots, $P < 0.05$). (f) Representative images acquired by confocal microscopy of mitochondria from 5-d-old root cells of WT, *cytc-1a*, 35S::GFP-TOR, and 35S::GFP-TOR \times *cytc-1a* seedlings grown as indicated in (a) and stained with the mitochondrial marker MitoTracker Green (1 μ M). Bars, 25 μ m. (g) Quantification of the MitoTracker Green fluorescence intensity observed in (f). Bars represent the mean (\pm SD) of the mean gray value, analyzed with Fiji software on equal areas of different roots ($n > 12$ roots). ns, not significant. (h) Quantification of total ATP content (nmol g^{-1} FW) measured by high-performance liquid chromatography (HPLC) in 4-d-old seedlings grown and treated with sucrose as indicated in Fig. 1(e). Bars represent mean (\pm SD). Different letters indicate significant differences based on Tukey's test (three biological replicates, $P < 0.05$).

(a) Normal conditions



(b) CYTc deficiency

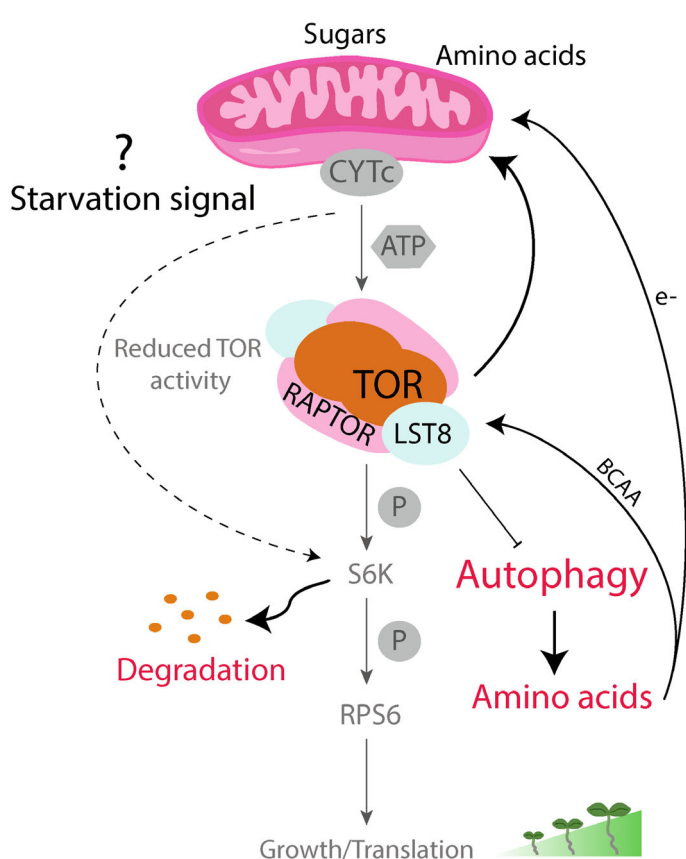


Fig. 7 Communication signals between mitochondria and the target of rapamycin (TOR) pathway. (a) Under normal growth conditions, mitochondria are fueled by specific molecules like sugars and amino acids, producing ATP through the electron transport chain pathway mediated by cytochrome *c* (CYTc). ATP and/or other unknown potential signals related to mitochondrial function (?) activate the TOR pathway and its downstream-regulated processes (inhibition of autophagy, S6K phosphorylation, RPS6 phosphorylation, translation), thus promoting growth. Autophagy-derived amino acids (BCAA) can regulate the TOR pathway and may serve as a mitochondrial electron source (e^-) (Cao *et al.*, 2019; O'Leary *et al.*, 2020). Alternatively (dashed arrow), the mitochondrial respiratory pathway controlled by CYTc can also modulate S6K levels, either directly or indirectly through TOR. Conversely, TOR can regulate mitochondrial function positively or negatively, maintaining ATP levels and affecting carbon metabolism (Cunningham *et al.*, 2007; Ramanathan & Schreiber, 2009; O'Leary *et al.*, 2020; Dai *et al.*, 2022). (b) The reduction in CYTc levels affects ATP levels and TOR-pathway activity, leading to a significant decrease in S6K, P-S6K, and P-RPS6 levels, resulting in a sharp decline in growth. Furthermore, the altered mitochondrial activity triggered by CYTc deficiency activates a 'starvation' alarm signal that causes an increase in the levels of autophagy and free amino acids, leading to a better adaptation to carbon-deficient conditions. Black lines, active pathway; gray lines, inhibited pathway; solid lines, demonstrated or previously reported evidence; dashed lines, proposed hypotheses. BCAA, branched-chain amino acids; e^- , electrons; ?, unknown signals; P, phosphorylation.

Mitochondrial bioenergetics and ATP production have been found to affect TOR activity in mammals, as reported by Kim *et al.* (2013). Meanwhile, evidence for a connection between mitochondrial activity and the TOR pathway in plants was initially obtained from the use of different types of OXPHOS inhibitors, showing that they prevented TOR activation by glucose (Xiong *et al.*, 2013; Zhang *et al.*, 2019; Wang *et al.*, 2020; Riegler *et al.*, 2021; Dai *et al.*, 2022). In addition, Brunkard *et al.* (2020) studied *increased size exclusion limit 3 (ise3)* mutant plants, lacking a mitochondrial protein, that shows altered transport across plasmodesmata. While loss-of-function of *ISE3* causes embryo lethality, deficient TOR activation was observed when *ISE3* was post-transcriptionally silenced using VIGS in Arabidopsis leaves. Even if these studies suggested the requirement of an active mitochondrial OXPHOS system for TOR activation, the use of chemical agents and VIGS may cause side effects due to unspecific inhibition of other cellular processes. More importantly, the conditions employed do not allow the discrimination between situations in which mitochondrial function is severely affected, and more 'physiological' situations in which changes in mitochondrial function are compatible with plant growth and development. Our study shows that a deficiency in an electron transporter directly involved in mitochondrial respiration and energy supply affects TOR activity, and this is the leading cause of the observed changes in plant growth and metabolism caused by this deficiency.

In addition to lower S6K and RPS6A phosphorylation, we observed a significant decrease in S6K protein levels in *cytc-1* mutant plants even when the *CaMV35S* promoter drives its expression (Fig. 4c). We hypothesize that lower ATP levels resulting from the altered mitochondrial activity post-transcriptionally affect S6K protein stability (Fig. 4g,h), significantly reducing S6K levels in various tissues and across different developmental stages (Fig. 4e,f). It is worth asking whether lower levels of mitochondrial activity primarily reduce TOR-pathway activation, thus resulting in lower S6K protein levels, or whether S6K levels are directly affected by changes in mitochondrial activity. Regarding these two possible scenarios, the P-S6K levels are only slightly decreased in *cytc-1* mutant plants after equalizing the S6K protein amount (Fig. 4d). However, this does not rule out the possibility that the reduced levels of S6K and P-S6K are due to a decrease in TOR activity, since our experiments with the 35S::GFP-TOR line demonstrated that high levels of TOR normalized S6K and P-S6K levels (Figs 5, 6). This may indicate that the decrease in S6K levels may also be a consequence of lower TOR activity. On the other hand, increasing TOR levels in the *cytc-1* mutant background, without recomposing mitochondrial activity and ATP content, recovers S6K protein levels (Fig. 5f).

This suggests that the reduced TOR activation signals S6K protein degradation. However, this reduction in S6K protein levels has not been previously reported in mutant plants with reduced TOR activation (Van Leene *et al.*, 2019; Zhang *et al.*, 2019; Scarpin *et al.*, 2020; Dai *et al.*, 2022), with a possible exception of experiments in which *ISE3*, notably encoding a mitochondrial protein, was silenced (Brunkard *et al.*, 2020). As previously suggested by Brunkard *et al.* (2020), decreased S6K

levels may be a consequence of a sustained decrease in TOR activity, affecting its stability. It is noteworthy that inhibition of the proteasome activity led to a substantial increase in both endogenous S6K and S6K-HA levels in the *cytc-1* mutant background (Fig. 4g,h). Additionally, the inhibition of vacuolar protein degradation in autophagic bodies by ConcA also significantly increased total S6K protein levels (Fig. 4h), suggesting that S6K could be degraded by autophagy. Increased S6K degradation may then be the result of autophagy activation in CYTc-deficient plants and possibly other plants with reduced TOR activity. Nevertheless, we did not detect significant changes in the levels of the S6K-target RPS6, suggesting that not all proteins undergo similar degradation routes.

A recent study also suggested that the TOR pathway plays a crucial role in regulating mitochondrial respiration and metabolism, deciding the final fate of amino acids between catabolism and energy production through respiration or anabolic routes through protein synthesis (O'Leary *et al.*, 2020). This study proposed that, in plants, certain amino acids activate TOR to affect the balance between catabolic and anabolic pathways, similar to observations made in animals. In our case, however, lower TOR-pathway activity was observed in CYTc-deficient plants even if they have a higher free amino acid content, suggesting a disconnection between amino acids levels and TOR-pathway activation, probably because the mitochondrial activity is required for TOR activation by amino acids in plants. Furthermore, it was shown that RAPTOR1b is localized in mitochondria, and both ATP levels and mitochondrial membrane potential are reduced in *raptor1b* mutants or plants exposed to AZD (Dai *et al.*, 2022). Similarly, in mammals, TOR localizes close to the outer mitochondrial membrane and interacts directly with proteins located on or near mitochondria to affect mitochondrial function (Ramanathan & Schreiber, 2009). It was documented that TOR stimulates mitochondrial functions by modulating the transcription of mitochondrial protein genes located in the nucleus, as well as controlling the translation of mitochondrial ribosomal proteins and components of respiratory Complexes I and V (Cunningham *et al.*, 2007). It has been suggested that regulating mitochondrial protein translation may be a common pathway used by TOR to control mitochondrial functions in mammals and plants (Scarpin *et al.*, 2020). These results establish a physical and functional link between the TOR complex and mitochondria, where the TOR pathway can positively or negatively regulate the function of mitochondria and control ATP levels. Regarding this, we observed that *raptor1b*, *rps6b*, and *lst8-1* mutants show increased CYTc protein levels (Fig. S8a), in agreement with the global proteomic study performed by Montes *et al.* (2022). CYTc levels play a relevant role in coordinating plant growth, as lack and overexpression of CYTc significantly affect plant growth rate and biomass production (Welchen & Gonzalez, 2016; Racca *et al.*, 2018). However, we could not reverse the growth phenotype of *raptor1b* and *rps6b* mutants by increasing CYTc expression (Fig. S8b–d), showing that an active TOR pathway is required for the growth-enhancing effect of CYTc in plants. On the other hand, even if TOR overexpression was able to restore growth and suppress other characteristics

carbon starvation (Broda *et al.*, 2018; Kacprzak & Van Aken, 2022), is basally activated in *cytc-1* mutant plants. Studies of these processes in CYTc-deficient plants would help to further dissect the molecular mechanisms involved in adjusting growth, metabolism, and stress responses to changes in mitochondrial activity.

In summary, we hypothesize that subtle mitochondrial dysfunction or fluctuations in mitochondrial activity affecting energy production are communicated to the rest of the cell through changes in TOR activity, which adjusts growth and metabolism accordingly. Meanwhile, more severe dysfunctions that block electron transport and cause an increase in ROS levels are transduced through the ANAC017 pathway to cope with this stressful situation. It would also be interesting to analyze possible connections between both pathways to further understand how mitochondrial activity connects to the rest of the cell, thus affecting growth and stress responses.

The authors thank Dr Jen Sheen (Dept. of Mol. Biol.-Massachusetts General Hospital, Dept. of Genetics-Harvard Medical School), Dr Lyuba Ryabova (Institut de Biologie Moléculaire des Plantes, Strasbourg, France) and Dr Pablo Manavella (IAL, Santa Fe, Argentina), as well as the ABRC (Ohio State University, USA), for providing seeds of different lines used in this study. We specially thank Dr Monica Mattio for help and technical assistance for ATP and amino acid determination by HPLC, and Lic. Tomas Tognetti for carbohydrates quantification. This work was supported by grants from ANPCyT (Agencia Nacional de Promoción Científica y Tecnológica, Argentina) PICT2018-1439, PICT2019-0310, PICT2020-0362, PICT2021-0486, CONICET (Consejo Nacional de Investigaciones Científicas y Técnicas, Argentina) and Universidad Nacional del Litoral (CAI+D2020). CMF is funded by the Max Planck Society (Partner Group for Plant Biochemistry). DEG, CMF, EW, and DHG are members of CONICET. MVC, NM, and AI are CONICET fellows.

None declared.

MVC, NM, DEG, AI and CMF performed the experiments and analyzed the data. MVC made the experiments, prepared the figures and wrote part of the manuscript. MVC, NM, CMF, DHG and EW participated in the discussion of the results. DHG and EW conceived the work, analyzed the data, and wrote the manuscript.

María Victoria Canal <https://orcid.org/0009-0003-7726-395X>

Carlos M. Figueroa  <https://orcid.org/0000-0003-4047-0480>
 Daniel H. Gonzalez  <https://orcid.org/0000-0002-3137-8095>
 Diana E. Gras  <https://orcid.org/0009-0000-0874-1995>
 Agustín Ibarra  <https://orcid.org/0009-0000-0690-6813>
 Natanael Mansilla  <https://orcid.org/0000-0001-6052-3223>
 Elina Welchen  <https://orcid.org/0000-0003-4025-573X>

Data availability

The data that support the findings of this study are available in the [Supporting Information](#) of this article.

References

- Artins A, Urrea-castellanos R, Martin-sánchez M, Moraes A, Fernie AR, Satake A, Caldana C. 2023. FCS-like zinc finger 14 (FLZ14) mediates the crosstalk between TORC and SnRK1 in response to sugar availability. *bioRxiv*. doi: [10.1101/2023.08.14.553285](https://doi.org/10.1101/2023.08.14.553285).
- Baena-González E, Hanson J. 2017. Shaping plant development through the SnRK1–TOR metabolic regulators. *Current Opinion in Plant Biology* 35: 152–157.
- Bantan-Polak T, Kassai M, Grant K. 2001. A comparison of fluorescamine and naphthalene-2,3-dicarboxaldehyde fluorogenic reagents for microplate-based detection of amino acids. *Analytical Biochemistry* 297: 128–136.
- Bassham DC. 2015. Methods for analysis of autophagy in plants. *Methods* 75: 181–188.
- Belda-Palazón B, Costa M, Beeckman T, Rolland F, Baena-González E. 2022. ABA represses TOR and root meristem activity through nuclear exit of the SnRK1 kinase. *Proceedings of the National Academy of Sciences, USA* 119: e2204862119.
- Broda M, Millar AH, Van Aken O. 2018. Mitophagy: a mechanism for plant growth and survival. *Trends in Plant Science* 23: 434–450.
- Brunkard JO, Xu M, Regina Scarpin M, Chatterjee S, Shemyakina EA, Goodman HM, Zambryski P. 2020. TOR dynamically regulates plant cell-cell transport. *Proceedings of the National Academy of Sciences, USA* 117: 5049–5058.
- Caldana C, Li Y, Leisse A, Zhang Y, Bartholomaeus L, Fernie AR, Willmitzer L, Giallisco P. 2013. Systemic analysis of inducible target of rapamycin mutants reveal a general metabolic switch controlling growth in *Arabidopsis thaliana*. *The Plant Journal* 73: 897–909.
- Cao P, Kim S-J, Xing A, Schenck CA, Liu L, Jiang N, Wang J, Last RL, Brandizzi F. 2019. Homeostasis of branched-chain amino acids is critical for the activity of TOR signaling in *Arabidopsis*. *eLife* 8: e50747.
- Charrier B, Champion A, Henry Y, Kreis M. 2002. Expression profiling of the whole *Arabidopsis* shaggy-like kinase multigene family by real-time reverse transcriptase-polymerase chain reaction. *Plant Physiology* 130: 577–590.
- Chen GH, Liu MJ, Xiong Y, Sheen J, Wu SH. 2018. TOR and RPS6 transmit light signals to enhance protein translation in deetiolating *Arabidopsis* seedlings. *Proceedings of the National Academy of Sciences, USA* 115: 12823–12828.
- Cunningham JT, Rodgers JT, Arlow DH, Vazquez F, Mootha VK, Puigserver P. 2007. mTOR controls mitochondrial oxidative function through a YY1-PGC-1 α transcriptional complex. *Nature* 450: 736–740.
- Dai L, Wang B, Wang T, Meyer EH, Kettel V, Hoffmann N, McFarlane HE, Li S, Wu X, Picard KL *et al.* 2022. The TOR complex controls ATP levels to regulate actin cytoskeleton dynamics in *Arabidopsis*. *Proceedings of the National Academy of Sciences, USA* 119: 1–12.
- De Clercq I, Vermeirssen V, Van Aken O, Vandepoele K, Murcha MW, Law SR, Inzé A, Ng S, Ivanova A, Rombaut D *et al.* 2013. The membrane-bound NAC transcription factor ANAC013 functions in mitochondrial retrograde regulation of the oxidative stress response in *Arabidopsis*. *Plant Cell* 25: 3472–3490.
- Dennis PB, Jaeschke A, Saitoh M, Fowler B, Kozma SC, Thomas G. 2001. Mammalian TOR: a homeostatic ATP sensor. *Science* 294: 1102–1105.
- Deprost DD, Yao L, Sormani RR, Moreau M, Leterreux G, Bedu MMM, Robaglia C, Meyer C, Nicolai M, Bedu MMM *et al.* 2007. The *Arabidopsis* TOR kinase links plant growth, yield, stress resistance and mRNA translation. *EMBO Reports* 8: 864–870.
- Dobrenel T, Mancera-Martínez E, Forzani C, Azzopardi M, Davanture M, Moreau M, Schepetilnikov M, Chicher J, Langella O, Zivy M *et al.* 2016. The *Arabidopsis* TOR kinase specifically regulates the expression of nuclear genes coding for plastidic ribosomal proteins and the phosphorylation of the cytosolic ribosomal protein S6. *Frontiers in Plant Science* 7: 1611.
- Figueroa CM, Lunn JE. 2016. A tale of two sugars: trehalose 6-phosphate and sucrose. *Plant Physiology* 172: 7–27.
- Forzani C, Duarte GT, Van Leene J, Clément G, Huguet S, Paysant-Le-Roux C, Mercier R, De Jaeger G, Leprince AS, Meyer C. 2019. Mutations of the AtYAK1 kinase suppress TOR deficiency in *Arabidopsis*. *Cell Reports* 27: 3696–3708.
- Gras DE, Mansilla N, Rodríguez C, Welchen E, Gonzalez DH. 2020. *Arabidopsis thaliana* SURFEIT1-like genes link mitochondrial function to early plant development and hormonal growth responses. *The Plant Journal* 103: 690–704.
- Hendriks J, Kolbe A, Gibon Y, Stitt M, Geigenberger P. 2003. ADP-glucose pyrophosphorylase is activated by posttranslational redox-modification in response to light and to sugars in leaves of *Arabidopsis* and other plant species. *Plant Physiology* 133: 838–849.
- Henriques R, Magyar Z, Bögre L. 2013. S6K1 and E2FB are in mutually antagonistic regulatory links controlling cell growth and proliferation in *Arabidopsis*. *Plant Signaling and Behavior* 8: e24367.
- Hildebrandt TM, Nunes Nesi A, Araújo WL, Braun HP. 2015. Amino acid catabolism in plants. *Molecular Plant* 8: 1563–1579.
- Ingarola C, Jéhanho I, Forzani C, Marmagne A, Broutin J, Clément G, Leprince A-S, Meyer C. 2023. The *Arabidopsis* target of rapamycin kinase regulates ammonium assimilation and glutamine metabolism. *Plant Physiology* 192: 2943–2957.
- Ivanova A, Law SR, Narsai R, Duncan O, Lee JH, Zhang B, Van Aken O, Radomiljac JD, van der Merwe M, Yi KK *et al.* 2014. A functional antagonistic relationship between auxin and mitochondrial retrograde signaling regulates alternative oxidase 1a expression in *Arabidopsis*. *Plant Physiology* 165: 1233–1254.
- Jamsheer M, Jindal S, Sharma M, Awasthi PSS, Sharma M, Mannully CT, Laxmi A. 2022. A negative feedback loop of TOR signaling balances growth and stress-response trade-offs in plants. *Cell Reports* 39: 110631.
- Kacprzak SM, Dahlqvist A, Van Aken O. 2020. The transcription factor ANAC017 is a key regulator of mitochondrial proteotoxic stress responses in plants. *Philosophical Transactions of the Royal Society B: Biological Sciences* 375: 20190411.
- Kacprzak SM, Van Aken O. 2022. Carbon starvation, senescence and specific mitochondrial stresses, but not nitrogen starvation and general stresses, are major triggers for mitophagy in *Arabidopsis*. *Autophagy* 18: 2894–2912.
- Kim SG, Hoffman GR, Poulgiannis G, Buel GR, Jang YJ, Lee KW, Kim BY, Erikson RL, Cantley LC, Choo AY *et al.* 2013. Metabolic stress controls mTORC1 lysosomal localization and dimerization by regulating the TTT-RUVBL1/2 complex. *Molecular Cell* 49: 172–185.
- Kühn K, Yin G, Duncan O, Law SR, Kubiszewski-Jakubiak S, Kaur P, Meyer E, Wang Y, Des Francs Small CC, Giraud E *et al.* 2015. Decreasing electron flux through the cytochrome and/or alternative respiratory pathways triggers common and distinct cellular responses dependent on growth conditions. *Plant Physiology* 167: 228–250.
- Li X, Cai W, Liu Y, Li H, Fu L, Liu Z, Xu L, Liu H, Xu T, Xiong Y. 2017. Differential TOR activation and cell proliferation in *Arabidopsis* root and shoot apices. *Proceedings of the National Academy of Sciences, USA* 114: 2765–2770.
- Liao CY, Pu Y, Nolan TM, Montes C, Guo H, Walley JW, Yin Y, Bassham DC. 2023. Brassinosteroids modulate autophagy through phosphorylation of RAPTOR1B by the GSK3-like kinase BIN2 in *Arabidopsis*. *Autophagy* 19: 1293–1310.
- Liu Y, Bassham DC. 2010. TOR is a negative regulator of autophagy in *Arabidopsis thaliana*. *PLoS ONE* 5: e11883.

- Liu Y, Duan X, Zhao X, Ding W, Wang Y, Xiong Y. 2021. Diverse nitrogen signals activate convergent ROP2-TOR signaling in Arabidopsis. *Developmental Cell* 56: 1283–1295.
- Lutt N, Brunkard JO. 2022. Amino acid signaling for TOR in eukaryotes: sensors, transducers, and a sustainable agricultural fuTore. *Biomolecules* 12: 387.
- Mahfouz MM, Kim S, Delauney AJ, Verma DPS. 2006. Arabidopsis TARGET OF RAPAMYCIN interacts with RAPTOR, which regulates the activity of S6 kinase in response to osmotic stress signals. *Plant Cell* 18: 477–490.
- Mair A, Pedrotti L, Wurzinger B, Anrather D, Simeunovic A, Weiste C, Valerio C, Dietrich K, Kirchler T, Nägele T *et al.* 2015. SnRK1-triggered switch of bZIP63 dimerization mediates the low-energy response in plants. *eLife* 4: e05828.
- Margalha L, Confraria A, Baena-González E. 2019. SnRK1 and TOR: modulating growth–defense trade-offs in plant stress responses. *Journal of Experimental Botany* 70: 2261–2274.
- Menegollo M, Tessari I, Bubacco L, Szabadkai G. 2019. Determination of ATP, ADP, and AMP levels by reversed-phase high-performance liquid chromatography in cultured cells. *Methods in Molecular Biology* 1925: 223–232.
- Meyer EH, Welchen E, Carrie C. 2019. Assembly of the complexes of the oxidative phosphorylation system in land plant mitochondria. *Annual Review of Plant Biology* 70: 23–50.
- Montané MH, Menand B. 2013. ATP-competitive mTOR kinase inhibitors delay plant growth by triggering early differentiation of meristematic cells but no developmental patterning change. *Journal of Experimental Botany* 64: 4361–4374.
- Montes C, Wang P, Liao CY, Nolan TM, Song G, Clark NM, Elmore JM, Guo H, Bassham DC, Yin Y *et al.* 2022. Integration of multi-omics data reveals interplay between brassinosteroid and target of rapamycin complex signaling in Arabidopsis. *New Phytologist* 236: 893–910.
- Ng S, De Clercq I, Van Aken O, Law SR, Ivanova A, Willems P, Giraud E, Van Breusegem F, Whelan J. 2014. Anterograde and retrograde regulation of nuclear genes encoding mitochondrial proteins during growth, development, and stress. *Molecular Plant* 7: 1075–1093.
- Ng S, Ivanova A, Duncan O, Law SR, Van Aken O, De Clercq I, Wang Y, Carrie C, Xu L, Kmiec B *et al.* 2013. A membrane-bound NAC transcription factor, ANAC017, mediates mitochondrial retrograde signaling in Arabidopsis. *Plant Cell* 25: 3450–3471.
- Nicastro R, Brohé L, Alba J, Nüchel J, Figlia G, Kipschull S, Gollwitzer P, Romero-Pozuelo J, Fernandes SA, Lamprakis A *et al.* 2023. Malonyl-CoA is a conserved endogenous ATP-competitive mTORC1 inhibitor. *Nature Cell Biology* 25: 1303–1318.
- Nicastro R, Ruccia S, Michel AH, Stumpe M, Osuna GMG, Jaquenoud M, Kornmann B, de Virgilio C. 2021. Indole-3-acetic acid is a physiological inhibitor of TORC1 in yeast. *PLoS Genetics* 17: 1–21.
- O'Leary BM, Oh GKG, Lee CP, Millar AH. 2020. Metabolite regulatory interactions control plant respiratory metabolism via target of rapamycin (TOR) kinase activation. *Plant Cell* 32: 666–682.
- Pendergrass W, Wolf N, Pool M. 2004. Efficacy of MitoTracker Green and CMXRosamine to measure changes in mitochondrial membrane potentials in living cells and tissues. *Cytometry. Part A: The Journal of the International Society for Analytical Cytology* 61: 162–169.
- Racca S, Gras DE, Canal MV, Ferrero LV, Rojas BE, Figueroa CM, Ariel FD, Welchen E, Gonzalez DH. 2022. Cytochrome *c* and the transcription factor ABI4 establish a molecular link between mitochondria and ABA-dependent seed germination. *New Phytologist* 235: 1780–1795.
- Racca S, Welchen E, Gras DE, Tarkowská D, Turečková V, Maurino VG, Gonzalez DH, Tarkowska D, Tureckova V, Maurino VG *et al.* 2018. Interplay between cytochrome *c* and gibberellins during Arabidopsis vegetative development. *The Plant Journal* 94: 105–121.
- Ramanathan A, Schreiber SL. 2009. Direct control of mitochondrial function by mTOR. *Proceedings of the National Academy of Sciences, USA* 106: 22229–22232.
- Raveneau M, Benamar A, Macherel D. 2017. Water content, adenylate kinase, and mitochondria drive adenylate balance in dehydrating and imbibing seeds. *Journal of Experimental Botany* 68: 3501–3512.
- Riegler S, Servi L, Scarpin MR, Godoy Herz MA, Kubaczka MG, Venhuizen P, Meyer C, Brunkard JO, Kalyna M, Barta A *et al.* 2021. Light regulates alternative splicing outcomes via the TOR kinase pathway. *Cell Reports* 36: 109676.
- Salem MA, Li Y, Wiszniewski A, Gialvalisco P. 2017. Regulatory-associated protein of TOR (RAPTOR) alters the hormonal and metabolic composition of Arabidopsis seeds, controlling seed morphology, viability and germination potential. *The Plant Journal* 92: 525–545.
- Scarpin MR, Leiboff S, Brunkard JO. 2020. Parallel global profiling of plant tor dynamics reveals a conserved role for larp1 in translation. *eLife* 9: 1–34.
- Schäufelberger M, Galbier F, Herger A, de Brito Francisco R, Roffler S, Clement G, Diet A, Hörtensteiner S, Wicker T, Ringli C. 2019. Mutations in the Arabidopsis ROL17/isopropylmalate synthase 1 locus alter amino acid content, modify the TOR network, and suppress the root hair cell development mutant lrx1. *Journal of Experimental Botany* 70: 2313–2323.
- Schepetilnikov M, Makarian J, Srour O, Geldreich A, Yang Z, Chicher J, Hammann P, Ryabova LA. 2017. GTPase ROP2 binds and promotes activation of target of rapamycin, TOR, in response to auxin. *EMBO Journal* 36: 886–903.
- Schepetilnikov M, Ryabova LA. 2018. Recent discoveries on the role of tor (target of rapamycin) signaling in translation in plants. *Plant Physiology* 176: 1095–1105.
- Schmitt V, Van Aken O. 2023. Mitophagy: from the dark into the spotlight. *Molecular Plant* 16: 1487–1489.
- Schwarzländer M, König A-CC, Sweetlove LJ, Finkemeier I. 2012. The impact of impaired mitochondrial function on retrograde signalling: a meta-analysis of transcriptomic responses. *Journal of Experimental Botany* 63: 1735–1750.
- Sheen J. 2014. Master regulators in plant glucose signaling networks. *Journal of Plant Biology* 57: 67–79.
- Shi L, Wu Y, Sheen J. 2018. TOR signaling in plants: conservation and innovation. *Development* 145: dev160887.
- Stitt M, McC. Lilley R, Gerhardt R, Heldt H. 1989. Metabolite levels in specific cells and subcellular compartments of plant leaves. *Methods in Enzymology* 174: 518–552.
- Tao Z, Barker J, Shi SDH, Gehring M, Sun S. 2010. Steady-state kinetic and inhibition studies of the mammalian target of rapamycin (mTOR) kinase domain and mTOR complexes. *Biochemistry* 49: 8488–8498.
- Thompson AR, Doelling JH, Suttangkakul A, Vierstra RD. 2005. Autophagic nutrient recycling in Arabidopsis directed by the ATG8 and ATG12 conjugation pathways. *Plant Physiology* 138: 2097–2110.
- Toral-Barza L, Zhang WG, Lamison C, LaRocque J, Gibbons J, Yu K. 2005. Characterization of the cloned full-length and a truncated human target of rapamycin: activity, specificity, and enzyme inhibition as studied by a high capacity assay. *Biochemical and Biophysical Research Communications* 332: 304–310.
- Van Leene J, Han C, Gadeyne A, Eeckhout D, Matthijs C, Cannoot B, De Winne N, Persiau G, Van De Slijke E, Van de Cotte B *et al.* 2019. Capturing the phosphorylation and protein interaction landscape of the plant TOR kinase. *Nature Plants* 5: 316–327.
- Voon CP, Guan X, Sun Y, Sahu A, Chan MN, Gardeström P, Wagner S, Fuchs P, Nietzel T, Versaw WK *et al.* 2018. ATP compartmentation in plastids and cytosol of *Arabidopsis thaliana* revealed by fluorescent protein sensing. *Proceedings of the National Academy of Sciences, USA* 115: 10778–10787.
- Wang Y, Qin Y, Li B, Zhang Y, Wang L. 2020. Attenuated TOR signaling lengthens circadian period in Arabidopsis. *Plant Signaling & Behavior* 15: 1710935.
- Welchen E, Canal MV, Gras DE, Gonzalez DH. 2021. Cross-talk between mitochondrial function, growth, and stress signalling pathways in plants. *Journal of Experimental Botany* 72: 4102–4118.
- Welchen E, García L, Mansilla N, Gonzalez DH. 2014. Coordination of plant mitochondrial biogenesis: keeping pace with cellular requirements. *Frontiers in Plant Science* 4: 551.
- Welchen E, Gonzalez DH. 2016. Cytochrome *c*, a hub linking energy, redox, stress and signaling pathways in mitochondria and other cell compartments. *Physiologia Plantarum* 157: 310–321.

- Welchen E, Gonzalez DH. 2021. Breaking boundaries: exploring short- and long-distance mitochondrial signalling in plants. *New Phytologist* 232: 494–501.
- Welchen E, Hildebrandt TM, Lewejohann D, Gonzalez DH, Braun HP. 2012. Lack of cytochrome c in Arabidopsis decreases stability of Complex IV and modifies redox metabolism without affecting Complexes I and III. *Biochimica et Biophysica Acta – Bioenergetics* 1817: 990–1001.
- Xiong Y, McCormack M, Li L, Hall Q, Xiang C, Sheen J. 2013. Glucose-TOR signalling reprograms the transcriptome and activates meristems. *Nature* 496: 181–186.
- Yang C, Li X, Yang L, Chen S, Liao J, Li K, Zhou J, Shen W, Zhuang X, Bai M *et al.* 2023. A positive feedback regulation of SnRK1 signaling by autophagy in plants. *Molecular Plant* 16: 1192–1211.
- Zhang N, Meng Y, Li X, Zhou Y, Ma L, Fu L, Schwarzländer M, Liu H, Xiong Y. 2019. Metabolite-mediated TOR signaling regulates the circadian clock in Arabidopsis. *Proceedings of the National Academy of Sciences, USA* 116: 25395–25397.

Supporting Information

Additional Supporting Information may be found online in the Supporting Information section at the end of the article.

Fig. S1 Evaluation of CYTc transcript and protein levels in *cytc-1* deficient plants.

Fig. S2 Mitochondrial retrograde response in *cytc-1* mutants.

Fig. S3 Starch and soluble sugar contents in *cytc-1a* mutant plants.

Fig. S4 Evaluation of the autophagy process in WT and CYTc-deficient plants.

Fig. S5 Evaluation of the autophagy in *atg5-1* × *cytc-1a* and *atg7-2* × *cytc-1b* plants.

Fig. S6 Transcriptional expression analysis of TOR-pathway components in *cytc-1* mutants.

Fig. S7 Analysis of the TOR-pathway activation in CYTc-deficient plants.

Fig. S8 High levels of CYTc do not restore growth in plants with reduced levels of TOR-pathway components.

Fig. S9 Original images used for Western blot analysis.

Fig. S10 Individual amino acid levels in 35S::GFP-TOR × *cytc-1a* plants.

Table S1 List of primer sequences used for qPCR analysis.

Please note: Wiley is not responsible for the content or functionality of any Supporting Information supplied by the authors. Any queries (other than missing material) should be directed to the *New Phytologist* Central Office.